High Harmonic Generation in Hollow Core Waveguides

Aaron von Conta

Master's Thesis

LUND UNIVERSITY

Faculty of Engineering
Department of Physics
2012

Anything worth doing, is worth doing right
Hunter S. Thompson

Abstract

The main goal of this thesis is to initiate a set of experiments on high-order harmonic generation (HHG) in hollow core waveguides and to verify a higher conversion efficiency of HHG in waveguides compared to classical HHG schemes.

High harmonics are in this context electromagnetic waves generated by focusing laser light into a dilute noble gas. The frequency of the thereby generated waves is q times larger than the frequency of the driving laser. Compared to second harmonic generation or third harmonic generation where q is 2 and 3, q in case of HHG can theoretically be up to a hundred or more. The obtained radiation, which is in the vacuum ultraviolet (VUV) and extreme ultraviolet (XUV) spectral regions, has a set of interesting properties which make it valuable for attosecond physics, classical spectroscopy and many more fields of physics.

Classically, a so-called free focusing geometry is used to generate high harmonics. This represents schematically just focusing the laser beam into a gas jet. Due to the absorption length of the harmonics at atmospheric pressure the whole setup, from generation, to interaction, to detection must be placed in vacuum. Using hollow core waveguides for the generation process results theoretically in a higher generation efficiency and better gas confinement in vacuum environment, therefore a higher conversion efficiency is expected.

Within this thesis a general theoretical foundation will be laid to understand the process of high harmonic generation and to explain the advantages of using hollow core waveguides. To underline the theoretical claims, a set of experiments is planned. The current status of the experiments is presented.

Contents

Chapter 1

Introduction

1.1 Prologue

It must have been some time around 1985 or 1986 [2, 3] when the phenomenon of high order harmonic generation (HHG) in gases was observed for the first time. All that was done, was to take a gas and available laser light with sufficient intensity and *puff* there were coherent x-rays (although it was not known at that point that they were coherent). The immediate question of *how* this was possible, was first answered in 1993 by the introduction of the semi classical three step model [8] and in 1994 a generally accepted quantum mechanical picture followed [4]. HHG has very much turned into a valuable scientific tool in the almost 20 years having past since then. Speaking in this context of a valuable scientific tool can be regarded an understatement. Attosecond light pulses [6] and thereby the whole field of attosecond physics [7] were products of the scientific aftermath of HHG.

From the earliest days on the output power of the generated harmonics was an important quantity. First to quantify the harmonics themselfs and later on for using them in other experiments. The conversion efficiency from the easily available laser light to the coherent XUV radiation was often the element deciding between a successful or failed experiment. It is therefore not surprising at all that propagation effects where already discussed in the very first publications after the general framework was available in 1994 [4, 5].
Phase-matching and phase control are the keywords in that respect. As early as 1998, hollow core waveguides were successfully used for phase matching purposes [9]. The research with regard to HHG in wave guiding structures has since then progressed steadily up to fairly recent demonstrations of sophisticated phase matching schemes in individually designed wave guides [34, 33].

Both HHG in general and high harmonic generation in hollow core waveguides in particular have been described and demonstrated over a decade ago. However, before the start of the project described in this work, the research group for attosecond physics in Lund had very limited experience in the use of hollow capillaries for HHG. The topic turned out to be a wonderful sand box full of mathematical, physical and technical challenges.

This first chapter contains as much physics with as little math as possible, in order to motivate the interested reader to actually go through the more complicated formalism presented in the following chapters. A rather phenomenological introduction to HHG is followed by a small chapter about the semi classical HHG picture, a short chapter introducing nonlinear optics and an introduction to wave guides. The whole introduction is kept in the style of a popular science text.

1.2 A Phenomenological Picture

1.2.1 What is HHG

HHG in the context of this thesis refers to the process of coherent XUV or VUV generation from laser light. The frequency of the generated radiation is q times larger than the frequency of the driving laser, whereas q can be theoretically up to a hundred or more. Experimentally there are different methods of creating such harmonics. Common is HHG from dilute nobel gases, where the light is interacting directly with atoms [2, 3] and a more complicated scheme of HHG from surfaces, where the light is interacting with with dielectric or metallic surfaces [10]. We will focus here on the solemnly on the first.

For HHG from noble gases typicall laser intensities of the order of $10^{14} \frac{W}{cm^2}$ are required.[1] Compared to an average nuclear powerplant with a continuous output power of giga (10^9) watts, these intensities are enormous. Experimentally these intensities are supplied by short pulsed lasers with pulse durations in the order of femtoseconds, yielding reasonable average output powers. Figure 1.1 depicts the process as explained above.

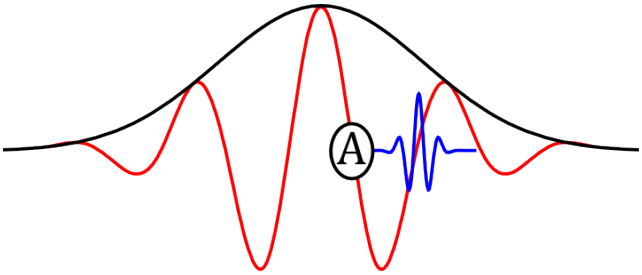

Figure 1.1: Phenomenological picture of HHG. An atom within a sufficiently strong electric light field emits radiation of higher frequencies. Experimentally the driving light field is usually a short light pulse.

1.2.2 Experimental considerations

An important point is, that due to the absorption length of the harmonics at atmospheric pressure the whole setup, from generation, to interaction, to detection must be placed in vacuum. This complicates the matter of making laser pulses and gas interact, as the handling of a gas source in vacuum can be delicate.

In this thesis two different possibilities for the field-gas interaction are considered. The classical case of a free focussing laser into a pulsed gas jet and the possibility of HHG in a hollow core waveguide. The two are displayed in figure 1.2. They have both distinct advantages and disadvantages that will be discussed in the later chapters.

1.3 The Process of HHG in Gases

1.3.1 The three step model

There is a very simple and straightforward model to explain HHG. It is called the semi classical three step model and was initially suggested by Paul Corkum [8]. Corkum stated that the process of creating high order harmonics can be divided in three distinct steps:

[1] This is explained by the onset of tunnel ionization in that region [11], how this is related will become clear later.

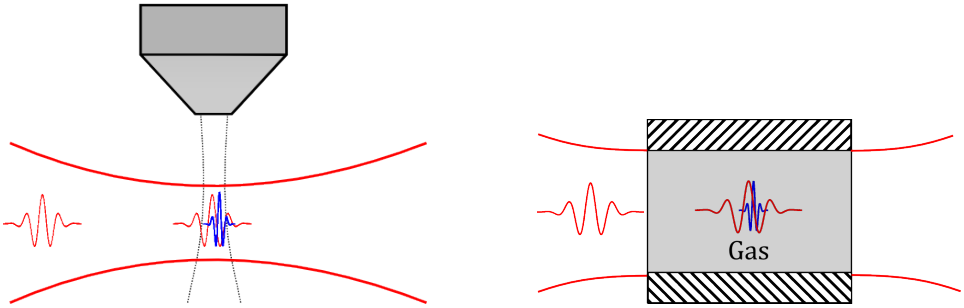

Figure 1.2: On the left HHG in a free focusing geometry, the gas is supplied via a pulsed gas jet. To the right HHG in a hollow core waveguide, the gas is distributed inside the waveguide.

1. The initially bound electron appears with zero velocity in the light field.
2. The electron is accelerated by the light field.
3. Re-colliding with the atom it is strongly decelerated, emitting radiation.

The first step is here the most complicated one to explain in an understandable manner. It would be necessary to consider the electron in a quantum mechanical manner and distinguish between several regimes depending on how strong the field is compared to the atomic potential. It is sufficient to know at this point that the electron can appear at several different times with respect to the external light field. This is due to inonization process being probabilistic in nature.

Once it is subjected to the external field, the motion of the electron is defined by the forces acting on it due to the light field.

Under certain circumstances the electron will then re-collide with the atom being almost instantaneously decelerated to zero velocity, therefore emitting its kinetical energy plus the binding energy in the form of electromagnetic radiation. An immediate deduction would be that the maximal photon energy can not exceed the electron energy at impact plus the ionization potential, due to the conservation of energy. Based on the three step model, very simple calculations reproducing characteristic features of HHG are possible.

1.3.2 Simulations based on the three step model

Figure 1.3 depicts simulations of the concept described above, assuming a cosine shaped linearly polarized electric field. The different black lines represent one dimensional trajectories of electrons that have appeared at different times in the electric field with the properties $y(t_0) = 0$, meaning that the atoms appear directly at the position of the atom and $v(t_0) = 0$, meaning that they have no initial velocity. Some of those electrons re-collide with the atom, in other words they come back to $y = 0$, while others wiggle away from the atom.
Above we deduced, that the maximal photon energy can not exceed the kinetic energy at impact plus the ionization potential. Plotting the kinetic energy of the simulated electrons at the re-impact on the atom (see figure 1.4), we find that our model predicts that

$$E_{photon-max} \leq 3.17U_p + I_p \tag{1.1}$$

Where U_p is the ponderomotive potential, that is in this case just a convenient way to collect factors like the electron charge, the electron mass, the light frequency etc. and I_p

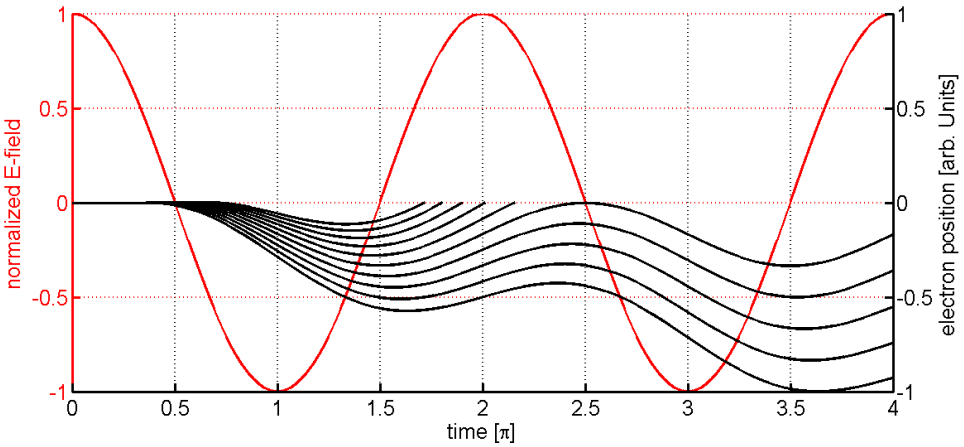

Figure 1.3: Different one-dimensional trajectories (black lines) for electrons appearing at different times in the external field (red line).

being the ionization potential.[2] This result agrees surprisingly well, with what has been measured in experiments (see for example figure 2.7). There is also only a small deviation from expressions obtained in more sophisticated models [15].

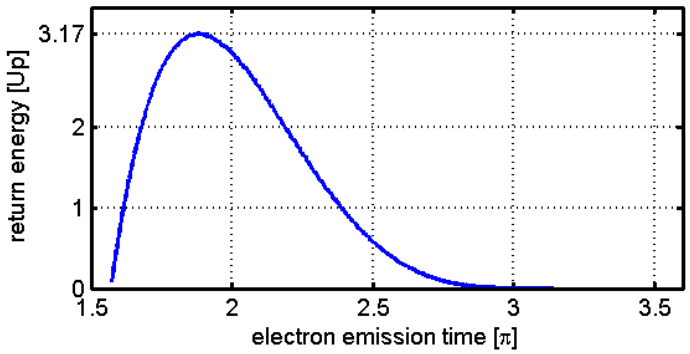

Figure 1.4: Kinetic energy at the re-impact on the atom for different electron emission times. The emission time is given in terms of multiples of π, representing the phase of the driving electric field $E \propto cos(t)$.

1.3.3 Shortcomings of the presented picture

In the way it was presented here the three step model does *not* include any information about either the process of the transformation of kinetical energy to electromagnetic radiation or about the phase of the generated light. This is due to the way it was narrated and not at all a shortcoming of the model. In the next chapter a fully quantum mechanical picture will be presented that includes all these informations and recreates the three step model as a special case. Therefore for all remaining questions the reader should be referred to the next chapter.

[2] However it can be shown in a straightforward manner that U_p represents the average kintetic energy of a free electron in a monochromatic light field.

1.4 Introduction to Nonlinear Optics

In order to explain HHG in a more general way and to ultimatively answer the questions at the end of the previous section the concept of nonlinear optics will be required.

1.4.1 Waves and harmonics

Thinking of light, the amplitude of the electromagnetic wave represents the brightness while the frequency represents the color. Now lets assume we have a box, that can do arbitrary mappings of a given light wave.

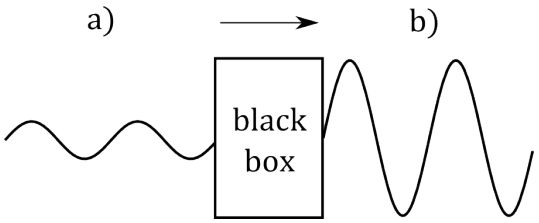

Figure 1.5: a) Ligth wave before a linear mapping and b) after a linear mapping. The difference is only in the amplitude of the two.

Consider a linear mapping of the input signal x on the output signal, defined by the relation $y = nx$. Physically, this just correspondings to scaling the input signal. It is depicted on the right side of figure 1.6. However if we have a mapping according to $y = x^2$, meaning that negative regions of the input signal are mapped onto positive values for the output signal it is clear that *the frequency and the color of the light must have changed*. This is depicted on the left side of figure 1.6.

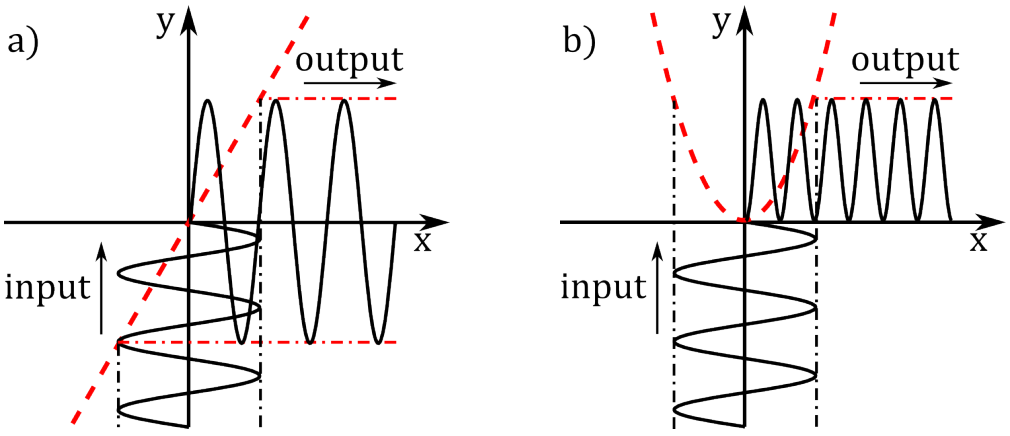

Figure 1.6: a) Shows a linear mapping of the input signal. b) Shows a quadratic mapping. Its clear that in case of the quadratic mapping the output signal must have frequency components of two times the input frequency.

It can be easily shown that if there is such a nonlinear process of $y \propto x^n$ that the output signal will contain frequency components of up to n times the input frequency [35]. These components are referred to as harmonics of n-th order. The next step is now to relate the thought above to light matter interaction.

1.4.2 The transition from linear to nonlinear optics

Thinking of an atom-electron system in terms of classical physics, the electron will sit in a minimum of the potential V. This minimum is an equilibrium position in the sense, that the electron will always return to it, if only perturbed slightly.

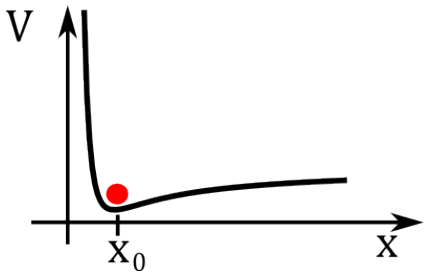

Figure 1.7: An example for an equivalent one-dimensional potential for attractive inverse-square law forces as expected when thinking about electron and atom in a classical way, the potential is then given by $V = a\frac{1}{x^2} - b\frac{1}{x}$ [25]. The electron sits in a minimum of the potential, being in an equilibrium position.

It will stay there as long as it has not enough energy to climb up the potential barrier, keeping it trapped. Taylor expanding the potential for the equilibrium position x_0 the first order term will vanish due to the nature of the minimum.

$$V = V_0 + \frac{1}{2}\frac{\partial^2}{\partial x^2}V(x)\bigg|_{x_0}(x-x_0)^2 + \frac{1}{6}\frac{\partial^3}{\partial x^3}V(x)\bigg|_{x_0}(x-x_0)^3 + \dots \tag{1.2}$$

Recalling from our very basic physics lectures that the force is given by minus the gradient of V we find that *closely around our equilibrium position* the force is linear with the displacement:

$$F = -\frac{\partial^2}{\partial x^2}V(x)\bigg|_{x_0}(x-x_0) \tag{1.3}$$

If we now consider putting the electron further and further away from x_0, the higher terms in the expansion will start to become important and expression 1.3 will gradually become inaccurate. In order to discuss the interaction of light with such a system, it is now necessary to introduce the concept of the polarization P.

The polarization is a quantity related to the electric dipole moment, which is nothing else but a measure of the separation of positive and negative electrical charges in a system of charges. A very simple definition for an one electron system would be $P = e(x - x_0)$. Meaning that the polarization is just the charge e times its deviation from the equilibrium position x_0. Recalling that an electric field E exerts per definition a force on a charge, it is intuitive that this quantity must describe how light, being an electric field, interacts with atoms, being a system of charges. The force on an electron due to the presence of an electric field with field strength E is given by:

$$F = eE \tag{1.4}$$

The relation between the force and the field is linear and from above we know that the relation between the force and the electron displacement is also linear. This implies that the polarization must go linearly with the strength of the electric field. Writing this as an equation:

$$P = \epsilon_0 \chi E \tag{1.5}$$

Where $\epsilon_0\chi$ is just the proportionality constant. However, this is only valid in the vicintiy of the equilibrium position, as otherwise the higher terms in the Taylor expansion must be included, adding higher order terms of E in equation 1.5. The final question that needs to be answered is, under which circumstances stays the electron closely to x_0? A very simple answer is, as long as the electric field of the light is very much smaller than the electric field of the atom at the equilibrium position. It turns out that the typical intensities needed to observe these effects on noble gas atoms are rarely achieved, that is why it is usually sufficient to work in the framework of linear optics. Linear refers here to the relation between electric field and polarization.

1.4.3 Nonlinear optics

It was discussed what happens if the electric field is small compared to the atomic field, however this thesis deals with exactly the opposite case. What happens if the electric field is comparable to the atomic fields. From what was said so far we would expect to see that the polarization is proportional to higher orders of E and that therefore the polarization will contain harmonic frequency components up to the highest order of E.

In order to realize what that means for the interacting light propagation, the basic physics lectures have to be recalled, where it was told that the generation of electromagnetic fields is related to a temporal change in the dipole moment. This was typically illustrated on the example of a simple antenna. In the introduction of the polarization it was said, that the polarization is a measure for the *atomic* dipole moment. Therefore, imagining the bound electrons around an atoms as tiny antennas, we expect not only harmonic frequency components in the polarization but also in the driving laser field. A formal introduction to the nonlinear polarization will follow in chapter 3.

1.5 Light Propagation in Waveguides

A waveguide is basically a structure that allows to contain a traveling wave. There is no limitation to light or electromagnetic waves in general, also acoustic waveguides exist. The most common waveguides are most probably the coaxial cable used for radio frequency transmission and the glass fiber used for transmission of light signals. *Contain* does not neccesarily mean that the light waves can not escape, as we will see in later chapters. Waveguides can also be lossy. It is more certain properties of the wave propagation inside the structure that defines a waveguide, what is meant by that will be more clear after this section.

In general, the behavior of light can be described at different levels of complexity, starting from ray or geometrical optics, to wave optics, to electromagnetic optics and finally quantum optics. These concepts became necessary for ever more detailed experimental observations. Some problems require the application of quantum optics while a large class of problems can be solved exactly in geometrical optics entirely without the other concepts. Propagation of light waves in waveguides can only be described in a satisfying manner dealing with electromagnetic optics, which is often very mathematical and inaccessible. However some properties of simple waveguides can be deduced in a rather intuitive way using a combination of geometrical and wave optics.

1.5.1 Properties of simple waveguides

The requirement for a waveguide was stated as containing a traveling wave. It can be interpreted as the condition, that the wave should reproduce itself inside the waveguide. The simplest geometry that could fulfill these requirements are two parallel perfect mirrors,

perfect in the sense of having 100% reflectivity. This geometry is often referred to as the planar mirror waveguide. Now thinking in terms of geometrical optics, the only parameters to describe a ray in two dimensions are its propagation angle α and a point on the ray. For our waveguide that requirement means that the input and output angle should be identical, which is true for all possible incoming angles if we think of an infinitely long waveguide.

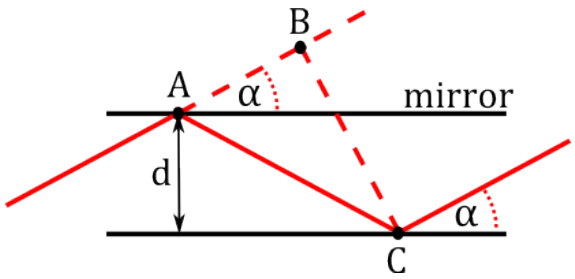

Figure 1.8: The planar mirror waveguide.

Things get complicated when we think in terms of waves. Looking at figure 1.8 it is clear that a beam leaving the wave guide will have a different phase at the output, unless the phase gain on the path $\overline{AB}$ equals the phase gain on the path $\overline{AC}$. This is called the condition of self consistency, being equivalent with the requirement, that the wave reproduces itself after a given distance. Mathematically it can be expressed as:

$$n\ 2\pi = \overline{AC} - \overline{AB} = 2\ k\ d\ \sin(\alpha_n) \tag{1.6}$$

The important thing here is, that not all possible beams fulfill this condition. Only for a defined combination of n and α_n the mirrors will be guiding. These distinct beams are usually referred to as modes of a waveguide, meaning fields fulfilling certain conditions that are maintained during the propagation in the waveguide. It is also intuitive, that these modes do have different properties than the normal free propagating light beam. In the example of the mirror waveguide from above the velocity with which a defined wavefront travels along the direction of the wave guide, is a factor $cos(\alpha_n)$ slower than in the free space. Therefore the wavenumber k inside the waveguide is different from the free space case and different from mode to mode.

1.5.2 Dealing with more complicated structures

The procedure from above cannot be extended to much more complicated structures, however two things derived above also apply for more complicated structures. There are certain field distributions called modes that reproduce themseves inside the waveguide. These modes travel with a different wavenumber inside the waveguide, accumulating a different phase each.

This property is what makes waveguides interesting for us, as the wavenumber and therefore the individual phase gain will be of central interest in the following chapters. The procedure of finding these modes can be cumbersome and there is no simple recipe to obtain those. In chapter 3 the derivation for a cylindrical waveguide is presented in great detail, from there the general path should be clearly evident. One of the waveguides that will be used in the experiment is displayed in figure 1.9.

1.6 Scope and Outline of this Work

The goal of this thesis was to investigate HHG in hollow core waveguides. Due to construction work at the laboratory and significant delay in a laser upgrade the

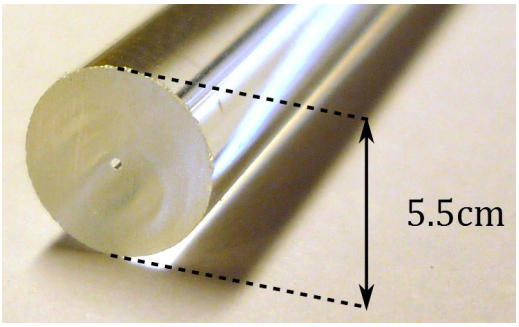

Figure 1.9: A heavy wall boro-silicate waveguide that will be used in the experiment. The core diameter of the pictured waveguide is 300 μm.

experiments planned could not be performed by the time this thesis needed to be handed in. As of that, this thesis mainly contains theoretical considerations on the matter and a small section about the current status of the experiment.

The theoretical part can be structured in two distinct sub sections. First, the description of the process of HHG on an atomic scale and second, calculations on the propagation effects in a waveguide. Both parts should provide the reader with a thorough picture of the individual processes and most importantly show how they are interacting. The goal of the two chapters chapters is to motivate the experiment.

Although the experiments were not conducted yet, all required items and calculations are presented. This includes a discussion of the general paradigm of the experiment, the to be used fibers, the constructed mounting system as well as calculations on the pressure dynamics inside the fiber.

Chapter 2

Single-Atom Response

2.1 Introduction to the Atomic Polarization

In the previous chapter it has been stated on a qualitative level how high harmonic generation is explained within the three step model. Anyhow the narration was chosen such that it is intuitive and simple. For instance, instead of saying the incident electromagnetic field distorts the Coulomb potential of the atom, thereby allowing parts of the electron wave function to reach the continuum through multi photon-, tunnel- or above threshold ionization. It was said an electron *appears* in the continuum. The following pages should now introduce the conceptual context and derive a model on a fully quantum mechanical basis. It can then be shown that in a special case this model reduces to the three step model.
The starting point here is something that has been hinted at already in the introduction, namely that the polarization $\vec{\mathcal{P}}(\omega)$ can be identified as a source term in the calculation of electric field propagation[1]. Therefore what needs to be found is a quantum mechanical description of the polarization of the single atom. It is convenient to start with the very simple model of an electron in a neutral atom. The polarization is then just given by

$$\vec{P}(t) = e\vec{x}(t) \tag{2.1}$$

Where $\vec{x}(t)$ is the displacement from the equilibrium position. Quantum mechanically $\vec{x}(t)$ is given by the expectation value of the x operator, or in Dirac notation

$$x(t) = \langle \Psi, t | \, x \, | \Psi, t \rangle \tag{2.2}$$

This basically *only* leaves us with the task of calculating $|\Psi, t\rangle$, or more explicitly finding the solutions of the Schrödinger equation for the given Hamiltonian of the system.

$$-i\hbar \frac{\partial}{\partial t} |\Psi, t\rangle = H \, |\Psi, t\rangle \tag{2.3}$$

The interaction Hamiltonian is here $H = H_0 + V_{light}(x, t)$, where H_0 denotes the Hamiltonian without the electromagnetic field. Solving the time dependent Schrödinger equation (eq. 2.3) (TDSE) exactly is a very tedious undertaking as for a real atom with a few electrons H_0 can be almost arbitrarily complicated. Therefore, as of today, exact solutions are only available in a very limited range of cases. Anyhow, there will be a short side note on these numerical TDSE calculations later in this text. What this chapter will focus on is a very intuitive set of approximations to the TDSE that allows us to properly explain the behavior of HHG in a reasonable region of experimental parameters.

[1] see chapter 3 for a more thorough discussion

2.2 Modeling the Electron Wave function

2.2.1 The single active electron approximation

As stated in the previous section, the first major source for complications is H_0 as it involves interaction terms among individual electrons. These interaction terms not only break the spherical symmetry but also couple the individual wave functions of the electrons. Equation 2.4 represents such a multi particle Hamiltonian for an i-electron system.

$$H_0 = \sum_i \left[\frac{p_i^2}{2m_i} + V_{nuc}(r_i) + \sum_{i \neq j} V_{i-j}(r_{ij}) \right] \tag{2.4}$$

In that expression the first term in the sum is just the kinetic energy of the i-th electron, the second term is the potential energy of the i-th electron due to the positive charges in the nucleus and the last term represents the interaction potential between the i-th and the j-th electron. There are now several strategies to circumvent the problems stated above while still maintaining a high degree of generality, notably the central field approximation [1]. Anyhow for simplicity we will choose none of these and go for the single active electron approximation. The complete Hamiltonian becomes then

$$H = \frac{p^2}{2m} + V_{eff}(r) + V_{light}(x,t). \tag{2.5}$$

In this case the effective core potential $V_{eff}(r)$ is chosen such that for the given atom the right ionization potential I_p is obtained. V_{light} denotes the potential exerted by the external light field that is needed for the following discussion.

2.2.2 Introduction of essential states

Now even with a single particle Hamiltonian the problem can still be quite complicated. For instance for the case of the single electron in a spherical symmetric potential the Schrödinger equation constitutes a Laplace equation, best written in spherical polar coordinates.

$$-i\hbar \frac{\partial}{\partial t} \Psi(r,\Theta,\Phi,t) = -\frac{\hbar^2}{2m} \Delta \Psi(r,\Theta,\Phi,t) + V(r) \Psi(r,\Theta,\Phi,t)$$

With the well known result that there is an infinite set of linearly independent solutions $\Psi(r,\Theta,\Phi,t)_{n,l}$ to this equation. The actual function describing the system may then be a linear superposition of these. Therefore the time evolution of the system is given by the individual time evolution of the infinitely many solutions. The concept becomes much more familiar if we refer to the individual solutions as individual states. In practice its often sufficient to consider only a few involved states. A good example for this is the two state formalism regularly used in laser theory or quantum information. There the total wave function is assumed to be of the shape $|\Psi\rangle = a\,|1\rangle + b\,|2\rangle$. Here a similar approach will be applied. It will be assumed that the electron is in its ground state $|0\rangle$ before the light is interacting with the atom. Further it couples from there directly into a continuum of momentum eigenstates $|b,p\rangle$ without occupying any non virtual intermediate states on the way there. Figure 2.1 depicts the choice of essential states.
Therefore the wave function is given in first order perturbation theory by

$$|\Psi,t\rangle = \exp\left(i\frac{I_p t}{\hbar}\right) \left[a(t)\,|0\rangle + \int b(p,t)\,|p\rangle\, dp^3 \right] \tag{2.6}$$

Where I_p denotes the ionization potential or the Eigen energy of $|0\rangle$. We have implicitly assumed, that the zero in energy is at the groundstate energy. A further simplification can

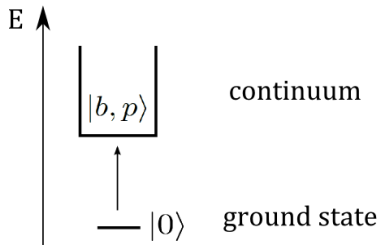

Figure 2.1: The essential states chosen for our model. A ground state $|0\rangle$ couples directly to a continuum of momentum Eigen states $|b,p\rangle$.

be applied by assuming that there is no depletion of the ground state population $a(t)$, respectively $a(t) = 1$. Within these approximation once the $b(p,t)$ are found the wave function is fully defined. The general way to achieve this is now to take the essential state wave function and plug it into the Schrödinger equation in order to find the function b(p,t).

$$-i\hbar\left[i\frac{I_p}{\hbar}\left(|0\rangle + \int b(p,t)\,|p\rangle\,dp^3\right) - \int \dot{b}(p,t)\,|p\rangle\,dp^3\right] = H\left[|0\rangle + \int b(p,t)\,|p\rangle\,dp^3\right] \tag{2.7}$$

Contracting the whole thing with $\langle p'|$ from the left and realizing that $\langle p'|\,0\rangle = 0$ this reduces to

$$-I_p b(p',t) + i\hbar\dot{b}(p',t) = \langle p'|\,H\,|0\rangle + \int b(p,t)\,\langle p'|\,H\,|p\rangle\,dp^3 \tag{2.8}$$

Although the essential state approximation is a strong approximation, in the sense that a lot of the atomic information given in the form of the additional bound states and Rydberg states is just discarded, it still yields results that show a lot of features that are observed in the experiment.

2.2.3 Slowly varying fields and the strong field approximation

The last thing to do here is to evaluate the two brackets in equation 2.8. This can be done by utilizing the strong field approximation [4]. It implies that the potential due to the presence of the electromagnetic radiation V_{light} is much stronger than the atomic potential once the electron has appeared in the continuum. Speaking in terms of the three step model, the electron appears in free space at high field intensities while it will return with a high kinetic energy. In both cases the atomic potential can be neglected. In fact it can be neglected all the time the electron travels in free space, as for $V_{light} \gg I_p$ the electron is expected to be far away from the atom. Therefore the atomic potential dropping with $\frac{1}{r}$ can be neglected. The Hamiltonian becomes

$$H = \frac{p^2}{2m} + V_{light}(x,t). \tag{2.9}$$

Another assumption that is needed to solve equation 2.8 analytically is that the envelope of the electric field does not vary much on the scale where the electron wavepacket travels. If that is the case we can assume that at every point in time the instantaneous field is approximately $E = \vec{E}_0\cos(\omega t)$. This is schematically depicted in figure 2.2. Taking multiple Å as the extend of the atom, as the order in which the electron wave packet moves, the pulse duration should be $\gg 10^{-19}$ s which is easily fulfilled by the femto second (10^{-15} s) pulses used for these kind of experiments.
The interaction potential becomes then:

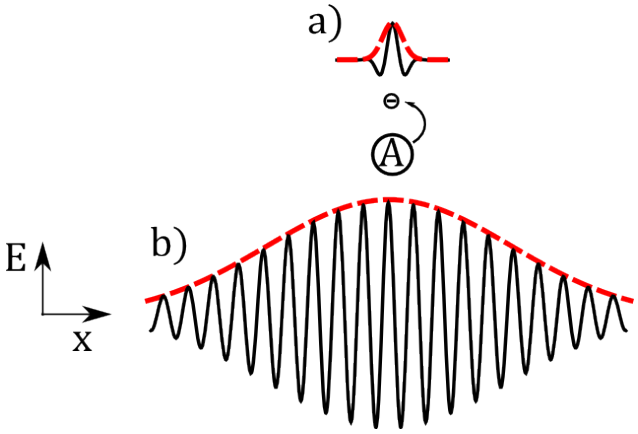

Figure 2.2: The figure shows the electric field of two pulses compared to the extend of the propagation of the electron wavefunction around an atom A. In a) the envelope function changes significantly on the scale of the path of the wave function, whereas in b) the change is way smaller. For long enough pulses the envelope function can be assumed as being constant.

$$V_{light}(x,t) = -xeE_0\cos(\omega t) \tag{2.10}$$

Therefore the final Hamiltonian has the form:

$$H = \frac{p^2}{2m} - xeE_0\cos(\omega t). \tag{2.11}$$

It has the very nice property that the momentum eigenstates are obviously eigenstates of the first part, while the second one leads to the well known and discussed dipole matrix element once plugged into equation 2.8.

$$\begin{aligned} -I_p b(p',t) + i\hbar\dot{b}(p',t) \;&=\; -eE_0\cos(\omega t)\,\langle p'|\,x\,|0\rangle + \\ &\quad \frac{p'^2}{2m}b(p',t) - eE_0\cos(\omega t)\int b(p,t)\,\langle p'|\,x\,|p\rangle\,dp^3 \end{aligned} \tag{2.12}$$

Using $\langle p'|\,x\,|p\rangle = i\hbar\frac{\partial}{\partial p}\delta_{pp'}$ allows us to write for $\dot{b}(p,t)$:

$$\dot{b}(p,t) = -i\frac{1}{\hbar}\left(\frac{p^2}{2m} + I_p\right)b(p,t) - eE_0\cos(\omega t)\frac{\partial}{\partial p}b(p,t) + \frac{ieE_0}{\hbar}\cos(\omega t)\,\langle p|\,x\,|0\rangle \tag{2.13}$$

This equation can be rewritten in a relativistic form by substituting the canonical momentum $\vec{\Pi}$ for the relativistic free electron in an external electromagnetic field [29] for the kinematic momentum used before.[2]

$$\vec{p} \equiv \vec{\Pi} = \vec{p} + e\vec{A} \tag{2.14}$$

Where p is, as before, the kinematic momentum and A is the vector potential. Equation 2.13 can then be cast into a closed form [4]:

$$\begin{aligned} b(p,t) \;&=\; i\int_0^t \frac{eE_0}{\hbar}\cos(\omega t')d_x\left(p + e\vec{A}(t) - e\vec{A}(t')\right)\times \\ &\quad \exp\left(-i\int_{t'}^t \frac{1}{\hbar}\left[\frac{1}{2m}\left(p + e\vec{A}(t) - e\vec{A}(t'')\right)^2 + I_P\right]dt''\right)dt' \end{aligned} \tag{2.15}$$

[2]The expression in Jackson [29] is in Gaussian units, here SI units are used.

The general path for doing the transition from equation 2.13 to 2.16 is to substitute $\frac{\partial b}{\partial p}$ by $\frac{\partial b}{\partial t}\frac{\partial t}{\partial p}$. Equation 2.16 can also be written in terms of the canonical momentum:

$$\begin{aligned} b(p,t) &= i\int_0^t \frac{eE_0}{\hbar}\cos(\omega t')d_x\left(\Pi - e\vec{A}(t')\right)\times \\ &\quad \exp\left(-i\int_{t'}^t \frac{1}{\hbar}\left[\frac{1}{2m}\left(\Pi - e\vec{A}(t'')\right)^2 + I_P\right]dt''\right)dt' \end{aligned} \tag{2.16}$$

$d_x(p)$ denotes here the dipole matrix element $\langle p|\, x\, |0\rangle$. With the vector potential for our linearly polarized laser field being defined as $\vec{E} = -\frac{\partial}{\partial t}\vec{A}$:

$$\vec{A} = \left(-\frac{E_0}{\omega}\sin(\omega t), 0, 0\right) \tag{2.17}$$

Therefore $b(p,t)$ can be calculated from experimentally available parameters and thus the wave function can be estimated. Equation 2.17 can also be written in a more compact way by introducing:

$$S(\Pi, t, t') = \int_{t'}^t \frac{1}{\hbar}\left[\frac{1}{2m}\left(\Pi - e\vec{A}(t'')\right)^2 + I_P\right]dt'' \tag{2.18}$$

The inner part of the integral can be identified as a Lagrangian of the free electron in a constant potential $-I_P$, which makes the whole integral the quasi classical action of the free electron propagation. If this analogy holds we would expect from a classical point of view that the extremal values of the action provide us with the actual motion of the electron. Anyhow this will be discussed at a later point in more detail. The to be evaluated expression for b(p,t) is at last:

$$b(p,t) = i\int_0^t \frac{eE_0}{\hbar}\cos(\omega t')d_x\left(\Pi - e\vec{A}(t')\right)\exp\left(-iS(\Pi,t,t')\right)dt' \tag{2.19}$$

2.3 Discussion of the Dipole Matrix Element

Having obtained a proper wave function, the next step is to substitute it in the definition of the dipole matrix element (given in equation 2.2).

$$x(t) = \left[\langle 0| + \int b^*\langle p|\, dp^3\right] x \left[|0\rangle + \int b\,|p'\rangle\, dp'^3\right] \tag{2.20}$$

This results in four separate matrix elements:

$$x(t) = \langle 0|\, x\, |0\rangle + \int b(t)\langle 0|\, x\, |p'\rangle\, dp'^3 + \int b^*(t)\langle p|\, x\, |0\rangle\, dp^3 + \int\int |b(t)|^2\langle p|\, x\, |p'\rangle dp'^3 dp^3 \tag{2.21}$$

The first term describes the coupling from the ground state to the ground state. Thinking of x in terms of creation and annihilation operators this term should vanish. Term number two and three are terms representing ground state-continuum coupling and the last term describes continuum-continuum coupling.

$$x(t) = x_{0-p}(t) + x_{p-0}(t) + x_{c-c}(t) \tag{2.22}$$

2.3.1 Continuum-continuum coupling

Upon generalizing the essential state model with regard to the parity of the continuum states, it can be shown that the dipole matrix element for continuum-continuum coupling must be null for all t. The generalization allows now, instead of one continuum with undefined properties, two continua $|b,p\rangle$ and $|c,p\rangle$ with different parity. This is convenient due to the dipole operator x being odd. Therefore all allowed transitions must involve both $|b,p\rangle$ and $|c,p\rangle$. Figure 2.3 depicts this model.

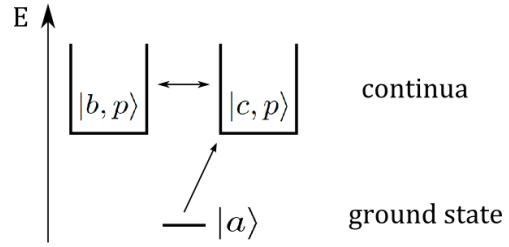

Figure 2.3: The essential states chosen for this argument. A groundstate $|a\rangle$ with a given parity and two continua $|b,p\rangle$ and $|c,p\rangle$ with different parity.

In this derivation, as only the qualitative result is sufficient, it will be assumed that $e = \hbar = c = 1$. Other than that, the rest of the derivation works in the same manner as in 2.2.2. The essential state wave function becomes:

$$|\Psi,t\rangle = \exp(i\frac{I_0}{\hbar}t)\left[a(t)\,|a\rangle + \int b(p,t)\,|b,p\rangle\,dp^3 + \int c(p,t)\,|c,p\rangle\,dp^3\right] \tag{2.23}$$

Introducing an interaction potential $V_i(t) = V_0 f(t)$, with the restriction that it couples $|a\rangle$ only to $|c\rangle$ the following three equations can be obtained by substituting equation 2.23 into the Schrödinger equation [12].

$$\begin{aligned}
\dot{a} &= -\frac{iV_0(t)}{2}\int c(p,t)dp \\
\dot{b} &= -ib(p,t) - iF(t)\int d(p,p')c(p,t)dp' \\
\dot{c} &= -ic(p,t) - \frac{iV_0(t)}{2}a(t) - iF(t)\int d(p,p')b(p,t)dp'
\end{aligned} \tag{2.24}$$

Where F(t) is the field coupling the two continuum states and $d(p,p')$ is the corresponding dipole matrix element. Under the assumption that the dipole matrix element is a symmetric function $d(p,p') = d(p',p)$ and using the wave function above in the definition of $x(t)$ given in equation 2.2, an expression for the continuum continuum contribution can be found.

$$x_{c-c}(t) = \int_{-\infty}^{+\infty}\int_{-\infty}^{+\infty} d(p,p')\left[b(p,t)c^*(p',t) + b^*(p,t)c(p',t)\right]dpdp' \tag{2.25}$$

It can be shown that $x_{c-c}(t)$ is zero for all t. Anyhow the argument is tricky. It can be shown [12] that if the initial values of $a(t)$, $b(p,t)$ and $c(p,t)$ fulfill certain symmetry conditions these symmetries are conserved in time. Explicitly if $a(t) = a^*(t)$, $b(-p,t) = -b^*(p,t)$ and $c(-p,0) = c^*(p,t)$ is fulfilled for $t = 0$ it will be fulfilled also at all later times.[3] The conditions, although initially looking complicated, are fulfilled by

[3]It can easily be shown for $a(t)$ by writing $a(t)$ and $a^*(t)$ in its explicit form, anyhow for the other two parameters its a bit more complicated.

$a(0) = 1$, $b(p,0) = c(p,0) = 0$ which are the usual starting parameters. Splitting the integrals $\int_{-\infty}^{+\infty} dp$ in equation 2.25 into $\int_{-\infty}^{0} dp + \int_{0}^{+\infty} dp$ and inserting the symmetries we find $x_{c-c}(t) = 0$.

2.3.2 A physical interpretation

The results of the previous section lead us to the conclusion that also in the calculation of the expectation value of $x(t)$ the $c - c$ terms can in general be neglected. Equation 2.22 becomes then

$$x(t) = x_{0-p}(t) + x^*_{p-0}(t) \tag{2.26}$$

Or more conveniently

$$x(t) = \int \left[b(t)\; d^*_x(p,t) + c.c. \right] dp^3. \tag{2.27}$$

Having the expression 2.27 for x(t) and having linked $b(t)$ to experimentally available parameters like the vector potential and the field strength, we can proceed to calculating x(t) explicitly.

$$x(t) = i \int_{-\infty}^{+\infty} \left[\int_0^t \frac{eE_0}{\hbar} \cos(\omega t') d_x \left(\Pi - e\vec{A}(t') \right) \times \right. \tag{2.28}$$
$$\left. d^*_x \left(\Pi - e\vec{A}(t) \right) \exp\left(-iS(\Pi, t, t') \right) dt' + c.c. \right] d\Pi^3$$

The different terms can now be interpreted according to [4, 21]. The first term in the integral $\frac{eE_0}{\hbar} \cos(\omega t') d_x \left(\Pi - e\vec{A}(t') \right)$ is the part of an electron wave packet to make the *transition to the continuum at time* t' with canonical momentum Π. $\exp\left(-iS(\Pi, t, t')\right)$ can be identified as the free space propagator, governing the phase gain of that part of the wave packet during propagation. Finally $d^*_x \left(\Pi - e\vec{A}(t) \right)$ describes the *recombination at time t*. This resembles the semi classical three step model described earlier anyhow with the distinction that we are considering and calculating all possible pathways for the electron wave packet. The possible interferences between these quantum paths distinguishes the two models, as for the semi classical case only *whole* electrons are propagated. The formulation here, talking of quantum paths and obtaining the final result by considering all possible pathways and weighting them acordingly, points very much in the direction of a Feynman path integral approach. Although not done here its worth pointing out that the problem can be fully treated in the path integral framework [22].

2.4 Estimating the Dipole Strength

In order to relate these considerations to possible experiments, it would be beneficial to further break down the expression obtained for the atomic dipole moment (eq. 2.29).

2.4.1 The saddle point approximation in 1-D

Switching the order of integration in equation 2.29, the integration in Π can be considered first. In doing so, *the different terms are evaluated in how fast they change with respect to the canonical momentum* Π. According to Lewenstein [4] the variation of the dipole moments in Π are much smaller than the variation of the quasi classical action. This leaves us with an equation of the type:

$$A = \int_{-\infty}^{+\infty} f(\vec{x}) e^{ig(\vec{x})} d^3x \tag{2.29}$$

In order to explain the mathematical method used for evaluating these kinds of equations its educative to consider the one dimensional case first, where

$$A_{1D} = \int_{-\infty}^{+\infty} f(x) e^{ig(x)} dx \tag{2.30}$$

With $f(x)$ and $g(x)$ being arbitrary functions having the only restriction that $g(x)$ varies much faster than $f(x)$. This allows us to exploit a mathematical tool called the saddle point approximation. Assuming that $f(x)$ is approximately constant on the scale of one oscillation of the exponential, the integration over that part will yield approximately zero. Therefore, the only regions where a significant contribution to the integral is expected are the regions around extrema of $g(x)$. Figure 2.4 depicts this behavior.

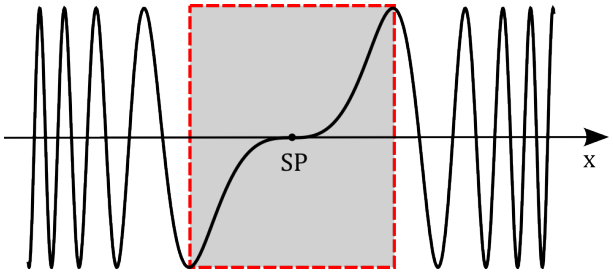

Figure 2.4: The principle of the saddle point approximation illustrated on the function $g(x) = sin(x^3)$ around zero. The major contribution to the integral $\int_{-\infty}^{+\infty} f(x)g(x)dx$ would come from the boxed region around the saddle point, as long as $f(x)$ changes slowly compared to g(x).

This can be exploited by Taylor expanding $g(x)$ in orders of x around the saddle point x_{SP} and truncating this expansion at second order.

$$g(x) = g(x_{SP}) + \frac{1}{2} g''(x_{SP})(x - x_{SP})^2 \tag{2.31}$$

The primes here denote the derivatives towards x, also the first derivative has disappeared as it was required for $g(x)$ to have an extremum at x_{SP}. Equation 2.30 becomes therefore

$$A_{1D} = \sqrt{\frac{2\pi}{ig''(x_{SP})}} f(x_{SP}) e^{ig(x_{SP})} \tag{2.32}$$

If there is a set of n saddle points and all of them are sufficiently far away from each other the thought above can easily be extended to match that case by just summing over the individual contributions.

$$A_{1D} = \sum_n \sqrt{\frac{2\pi}{ig''(x_{SP_n})}} f(x_{SP_n}) e^{ig(x_{SP_n})} \tag{2.33}$$

Its straight forward to extend this principle to three dimensions. All that need to be done is execute the integrations in the three spatial directions consecutively, each time using a 1D saddle point approximation. The only thing that changes then from the equation above is that the pre factor in the square root gets raised to the power of the considered dimensions. Anyhow that implies the assumption that $g''(x_{SP_n})_x = \frac{\partial^2}{\partial x^2} g(\vec{x})|_{\vec{x}_{SP}}$ equals $g''(x_{SP_n})_y$ and $g''(x_{SP_n})_z$.

$$A = \sum_n \left(\frac{2\pi}{ig''(x_{SP_n})} \right)^{\frac{3}{2}} f(x_{SP_n}) e^{ig(x_{SP_n})} \tag{2.34}$$

Applying this principle on $x(t)$ its helpful to write it in a convenient form before.

$$x(t) = i \int_0^{t'} \left[\int_{-\infty}^{+\infty} f(\Pi, t, t') \, \exp\left(-iS(\Pi, t, t')\right) d\Pi^3 \right] dt' + c.c. \tag{2.35}$$

Therefore analogously to equation 2.35

$$x(t) = i \int_0^{t'} \left[\sum_n \left(\frac{2\pi}{iS''(\Pi_{SP_n}, t, t')} \right)^{\frac{3}{2}} f(\Pi_{SP_n}, t, t') \, e^{-iS(\Pi_{SP_n}, t, t')} \right] dt' + c.c. \tag{2.36}$$

There are now two problems in interpreting expression 2.36. The first is how to find the saddle point in the first place and the second is how to interpret $S''(\Pi_{SP_n}, t, t')$. Anyhow latter is easily addressed as:

$$\begin{aligned} S''(\Pi_{SP_n}, t, t') &= \left[\frac{d^2}{d\Pi^2} \int_{t'}^{t} \frac{1}{\hbar} \left[\frac{1}{2m} \left(\Pi - e\vec{A}(t'') \right)^2 + I_P \right] dt'' \right]_{\Pi_{SP_n}} \\ &= \frac{1}{\hbar m} \int_{t'}^{t} 1 dt'' = \frac{\tau}{\hbar m} \end{aligned} \tag{2.37}$$

Additionally to that, t' can be substituted by $t' = t - \tau$ and therefore the integration changes from dt' to $-d\tau$. By doing so the integration boundaries can extended to cover $0 \leq \tau < \infty$ circumventing causality issues.

$$x(t) = i \int_0^{\infty} \left[\sum_n \left(\frac{2\pi\hbar m}{\epsilon + i\tau} \right)^{\frac{3}{2}} f(\Pi_{SP_n}, t, t') \, \exp\left(-iS\left(\Pi_{SP_n}, t, \tau\right)\right) \right] d\tau + c.c. \tag{2.38}$$

The additional ϵ term appearing in the saddle point prefactor is first of all a mathematical necessity to prevent the integral from diverging at $\tau = 0$. [4] The whole prefactor has a nice physical interpretation, being a factor accounting for quantum diffusion of the wave packet deposited to the continuum. This means, that while the electron wave packet travels in the continuum it expands, therefore, the longer it travels the smaller will be the overlap integral with the initial state wave function.

2.4.2 Saddle points of the quasi classical action

The saddle points of the quasi classical action are defined by the extrema of $S(\Pi, t, t')$ with respect to Π:

$$\nabla_\Pi \, S(\Pi_{SP_n}, t, t') = \nabla_\Pi \int_{t'}^{t} \frac{1}{\hbar} \left[\frac{1}{2m} \left(\Pi - e\vec{A}(t'') \right)^2 + I_P \right] dt'' = 0 \tag{2.39}$$

Further the nabla operator can be applied before the integral, as the initial canonical momentum Π is independent of t''. Therefore:

$$0 = \int_{t'}^{t} \frac{1}{m} \left(\Pi - e\vec{A}(t'') \right) dt'' \tag{2.40}$$

The expression in the integral represents now the particle momentum divided by the mass and corresponds to the particle velocity. Therefore the condition for the saddle point can be broken down to

$$0 = [r]_{t'}^{t} = r(t) - r(t') \tag{2.41}$$

Where $r(t)$ denotes the location of the electron at time t. This has a very nice interpretation, recalling from before that t' has been identified as the electron emission time. *The dominant contribution to the expectation value of $x(t)$ comes from the electrons being ejected from the nucleus but then re encounter it while traveling in the electromagnetic field.* Again the semi classical picture appears to be correct.

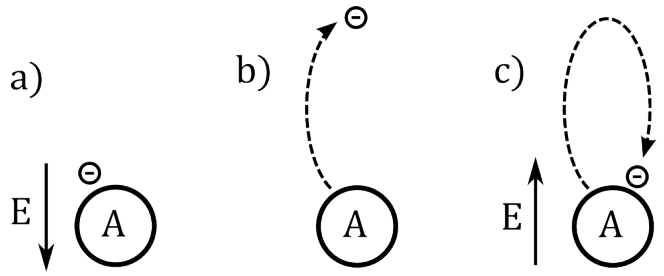

Figure 2.5: A possible quantum path contributing to the expectation value $x(t)$ of the dipole operator. a) At $t-\tau$ the part of the electron wave function is ejected into the continuum with a canonical momentum Π_{SP}. b) The electron wave packet propagates for a time period τ in the continuum. c) The wave packet comes back to its initial position at the time t.

Although the train of thought above did not directly add anything to the progress of calculating $x(t)$, the next few lines will show how the the physical insight gained about the character of t and t' and the boundary conditions in $r(t)$ and $r(t-\tau)$ can be used to estimate $S(\Pi_{SP-n}, t, t')$. What we are looking for is the momentum with which the electron is emitted into the continuum Π_{SP-n}. It can be obtained following a strictly classical consideration of the electron trajectory. Introducing the time of flight $\tau = t' - t$ we can write:

$$p_{st}(t) = \int_{t-\tau}^{t} F(t)dt + p_0 \tag{2.42}$$

In the beginning of these calculations (see 2.2.3) we assumed the electric field to be of the shape $F(t) = eE_0 cos(\omega t)$. It was shown above, that the boundary conditions at the saddle point are given by $r(t-\tau) = r(t) = 0$. Therefore equation 2.42 has to be integrated another time to obtain:

$$r(t) = \int_{t-\tau}^{t} \frac{p_{st}(t)}{m} dt = \left[-\frac{eE_0}{m\omega^2} cos(\omega t) + p_0 t + r_0 \right]_{t-\tau}^{t} \tag{2.43}$$

Implementing the boundary conditions that yields

$$\Pi_{SP} \approx p_0 = \frac{eE_0}{m\omega^2 \tau} \left[cos(\omega t) - cos(\omega(t-\tau)) \right] \tag{2.44}$$

Using the result above together with the explicit form of the vector potential given in equation 2.17 allows us to calculate the integral in the definition of the quasi classical action (eq. 2.18).

$$\begin{aligned} S_{SP}(t,\tau) &= \int_{t-\tau}^{t} \frac{1}{\hbar} \left[\frac{1}{2m} \left(\Pi_{SP} - e\vec{A}(t'') \right)^2 + I_P \right] dt'' \\ &= \frac{1}{\hbar} \left[I_p \tau + 2U_p \int_{t-\tau}^{t} \left(\frac{1}{\omega\tau} \left[\cos(\omega t) - \cos(\omega(t-\tau)) \right] + \sin(\omega t'') \right)^2 dt'' \right] \\ &= \frac{1}{\hbar} \left[(I_p + U_p)\tau - 2\frac{U_p}{\tau\omega^2} \left[1 - \cos(\omega\tau) \right] - \frac{U_p}{\omega} C(\tau) \cos\left(\omega[2t-\tau]\right) \right] \end{aligned} \tag{2.45}$$

Where the function $C(\tau)$ is defined as:

$$C(\tau) = \sin^2(\omega\tau) - \frac{4}{\tau\omega}\sin^2\left(\frac{\omega\tau}{2}\right) \tag{2.46}$$

Further it was made use of the ponderomotive potential $U_p = \frac{e^2E_0^2}{4m\omega^2}$. It is at this position important to point out that

$$U_p \propto E_0^2 \propto I_{Laser}, \tag{2.47}$$

as the laser intensity I_{Laser} will lateron be the quantity of interest in the discussion of the porpagation effects.

2.4.3 Modeling the dipole matrix elements.

The findings in the previous two sections, together with equation 2.29 culminate in equation 2.49.

$$x(t) = i\int_0^\infty \left[\sum_n \left(\frac{2\pi\hbar m}{\epsilon + i\tau}\right)^{\frac{3}{2}} \frac{eE_0}{\hbar}\ \cos\left(\omega[t-\tau]\right)\ d_x\left(\Pi_{SP-n}(t,\tau) - e\vec{A}(t-\tau)\right) \times \right. \tag{2.48}$$
$$\left. d_x^*\left(\Pi_{SP-n}(t,\tau) - e\vec{A}(t)\right)\exp\left(-iS_{SP-n}\left(t,\tau\right)\right)\right] d\tau + c.c.$$

It becomes clear at that point, that the only thing now missing is some model for the dipole matrix elements $d_x(\Pi)$ and $d_x^*(\Pi)$. The task itself is initially fairly straight forward. Pick a ground state wave function and calculate the overlap integral $\langle\Pi|\, x\,|0\rangle$ with the to be investigated momentum eigenstate. This is then the end of the part where the task pretends to be easy, as already the question of which ground state wave function to choose and how the momentum states are considered is problematic. For instance describing the electron momentum eigenstates in the presence of an electric field, becomes a conceptually nontrivial undertaking, if done relativistically correct (see [23]). In reference [4] the two simplest possible models are presented for a Gaussian ground state wave function and for Hydrogen-like atoms with plain wave states instead of the apropriate Volkow states as momentum eigenstates. Anyhow it would go beyond the scope of this thesis to present a deeper theoretical discussion on that matter. Quoting the solution for the Hydrogen-like atom in the limit $\hbar = \omega = m = 1$ [4, 24]:

$$d(\Pi) \approx i\left(\frac{2^{7/2}(2I_p)^{5/4}}{\pi}\right)\frac{\Pi}{\left(\Pi^2 + (2I_p)^2\right)^3} \tag{2.49}$$

For the further discussion its important to clarify that *dipole strength* refers to $\|(x(\omega))\|^2$. Figure 2.6 shows simulations of the dipole strength as a function of the harmonic order. The results resemble the features of hhg data obtained experimentally on suitable systems, an example of this data is displayed in figure 2.7. In particular the typical plateau with a cutoff at approximately $3.17U_p + I_p$ [18] can be observed, this result is also what was obtained in the introduction by completely classical calculations. A more detailed discussion of the model and the quality of the calculations will be omitted, as it would lead to far. For a thorough discussion the reader is referred to [22, 19, 18] and the references therein. It is sufficient for our purposes to have shown at this point, that the model we have chosen shows a qualitatively correct behavior and that it agrees, respectively deviates only slightly, from the predictions of the semi classical model.

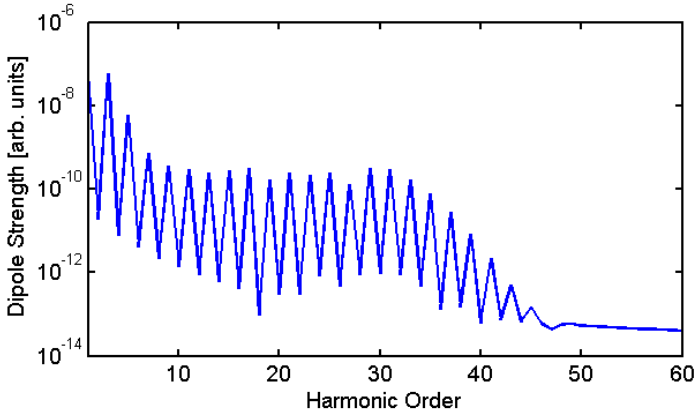

Figure 2.6: Simulation of the dipole strength $|x(\omega)|$ according to the model described in this section in the limit of $\hbar = \omega = m = e = \omega = 1$. The parameters are $U_p = 8$, $I_p = 5$.

2.4.4 The dipole phase of individual harmonics

This section contains now the second major item the whole chapter was working towards. The information about how the microscopic phase of the individual harmonics behaves with respect to the driving electromagnetic field. Although not immediately obvious this information is crucial for calculating the harmonic buildup (see the following chapter). In the current model there are only two experimentally accessible quantities assuming the type of atoms in consideration are fixed. The wavelength and the ponderomotive potential, whereas the latter is equivalent to the intensity of the driving field. Now focusing on the intensity dependence, the dipole strength and the atomic phase are calculated for different values of U_p. The term atomic phase is there referring to the argument of $x(\omega)$, it represents the phase gain in the whole process of emission, propagation and recombination of the free electron.
Picture 2.8 shows a typical result of these calculations. It is important to see that the atomic phase changes significantly compared to π even within small variations of the intensity, further the dependence of the atomic phase on the intensity seems to first order linear. This behavior is independent of the harmonic order. It seems apropriate to approximate the atomic phase as

$$\phi_{atomic} \propto \alpha U_p I_{light} \tag{2.50}$$

The question is how the atomic phase relates to the dipole phase, which is calculated relative to the incident electric field or more specifically to the generated harmonic at other points in space. Anyhow this discussion will be postponed until section 3.2.4.

2.5 Conclusion on Chapter 2

To briefly summarize the findings of this chapter: It was shown, that a very simple essential state model is sufficient to explain the qualitative behavior of HHG. In various positions of the derivation analogies between the quasi classical picture and this fully quantum mechanical picture can be found. This extends up to the point where the individual terms in the quantum mechanical representation of the dipole operator can be identified with the three steps suggested by Corkum.
The introduction, or more correctly identification, of the quasi classical action allows us to use its properties to predict the possible electron paths in the electromagnetic field and

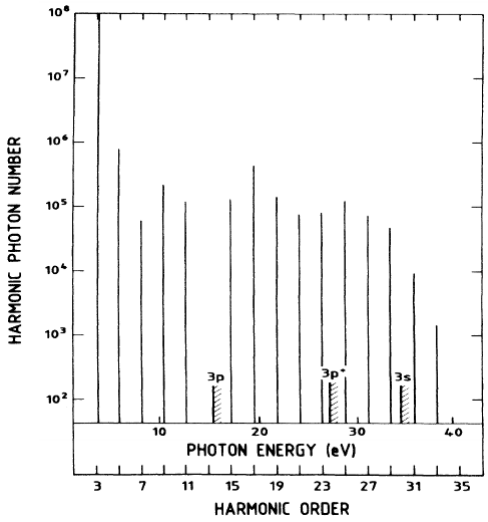

Figure 2.7: Harmonic-Intensity distribution in Ar at 3×10^{13} $\frac{W}{cm^2}$ and at 15 Torr pressure, together with the used wavelength of $\lambda = 1064\,\text{nm}$ this corresponds to $U_p \approx 5eV$. The first ionization potential I_p of Argon is at 15.8 eV [45]. Taken from reference [17].

thereby solving the required momentum integration in a saddle point approximation. In order to do so a brief introduction to this mathematical tool was given.
A basic qualitative calculation using the presented formalism was shown and compared with experimental data. It was finally found that the atomic phase of the high harmonics behaves approximately linearly with the ponderomotive potential exerted by the incident electromagnetic light. Therefore the atomic phase is approximately linearly dependent on the intensity. It is also important to stress that the change of dipole phase is large compared to π if the intensity doubles; this should be kept in mind for the following discussion.

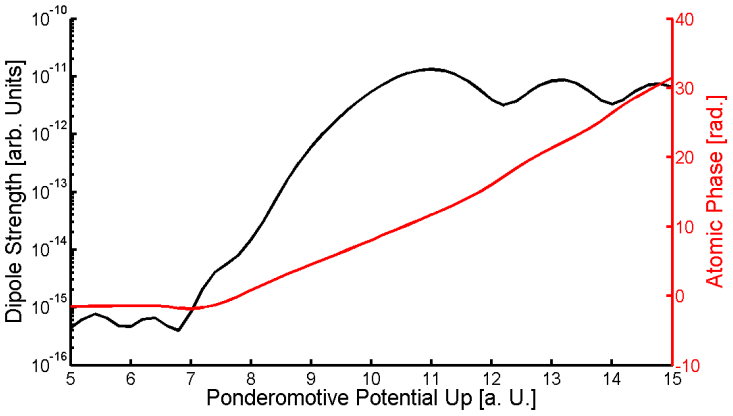

Figure 2.8: Dipole strength and atomic phase of the 35 harmonic as a function of U_p. The ionization potential was chosen to $I_p = 1.5$ which corresponds approximately to the value for argon in the given units.

Chapter 3

Propagation Equations and Phase Matching in Waveguides

3.1 Introduction to Propagation Equations

3.1.1 The general problem

It has been shown in the previous chapter that the atomic response to the incident radiation results in an intensity dependent phase and a dipole strength for a given harmonic order. In the second step of the theoretical description we have to direct our attention now towards the macroscopic propagation of the harmonic field. The crux of the biscuit is here to find solutions to the Maxwell equations that accurately describe the evolution while not getting too complicated to solve. The starting point for this is here the vectorial Helmholtz equation in time domain which can be directly obtained from the free space Maxwell equations (sketch of the derivation is given in 3.3.1).

$$\nabla^2 \vec{E} - \frac{1}{c^2}\frac{d^2}{dt^2}\vec{E} = \mu_0 \frac{d^2}{dt^2}\vec{P} \tag{3.1}$$

The next step is to transform this equation into frequency domain and introduce the usual expansion of $\vec{\mathcal{P}}$ in orders of $\vec{\mathcal{E}}$. Cursive letters shall denote here Fourier transformed quantities.

$$\nabla^2 \vec{\mathcal{E}} + \frac{\omega^2}{c^2}\vec{\mathcal{E}} = -\mu_0 \omega^2 \epsilon_0 \left[\chi^{(1)}\vec{\mathcal{E}} + (\chi^{(2)}\vec{\mathcal{E}})\vec{\mathcal{E}} + (\ldots)\right] \tag{3.2}$$

Where the quantities χ^n represent the n-th order dielectric susceptibility tensor. It is now useful to write total electric field as sum of the individual harmonics.

$$\vec{\mathcal{E}}(\vec{r},\omega) = \sum_q \vec{\mathcal{E}}_q(\vec{r},\omega) \tag{3.3}$$

Combining the above with equation 3.2 a set of q differential equations is obtained. The whole set is coupled due to the higher order terms in $\vec{\mathcal{E}}$.

3.1.2 Linearization and the Born approximation

The complexity of solving the wave equations is drastically reduced by keeping the equation linear in $\vec{\mathcal{E}}$ and assuming that the $\vec{\mathcal{E}_q}$ are not overlapping in frequency domain. Therefore we drop the terms of order greater than one in the power expansion of $\vec{\mathcal{P}}$ and reintroduce the coupling indirectly with an additional nonlinear polarization depending only on the fundamental.

$$\vec{\mathcal{P}}_q(\vec{r},w) = \epsilon_0 \chi_q^{(1)} \vec{\mathcal{E}}_q(\vec{r},w) + \vec{\mathcal{P}}_q^{NL}(\vec{\mathcal{E}}_F) \tag{3.4}$$

$\vec{\mathcal{E}}_F$ denotes there the electric field of the fundamental. This step might sound bold but has proven to be very useful in the past [13, 14, 16]. The propagation is then described for the q-th harmonic and the fundamental by the following set of equations:

$$\nabla^2 \vec{\mathcal{E}}_F + \frac{\omega^2}{c^2} n_F^2 \vec{\mathcal{E}}_F = 0 \tag{3.5}$$

$$\nabla^2 \vec{\mathcal{E}}_q + \frac{\omega^2}{c^2} n_q^2 \vec{\mathcal{E}}_q = -\frac{\omega^2}{\epsilon_0 c^2} \vec{\mathcal{P}}_q^{NL}(\vec{\mathcal{E}}_F) \tag{3.6}$$

Where we have made use of the fact that the linear refractive index is defined as $n_q^2 = 1 + \chi_q^{(1)}$. The fundamental is thus propagating just like in the case without harmonic generation. Unconsciously we made an approximation that is usually referred to as the Born approximation. It means that we are treating the Harmonics as a perturbation to the initial field. Therefore to first order the fundamental remains unchanged. It is also important to note that with this approach no interaction effects between the harmonics itself are included anyhow it can easily be extended to include for instance low order harmonics.
The general strategy to obtain a complete solution is then to compute first the propagation of the fundamental through the geometry. And then in a second step use the results to compute the propagation of the harmonic in question.

3.1.3 The free propagation case and the co-propagating frame

In the case of no present wave guiding geometry a laser pulse can be described as an envelope function times the plane wave function of the center frequency. Here a one dimensional case is considered

$$\vec{E}_F(\vec{r},t) = V_F(z,t)\, exp(i\omega_0 t) \tag{3.7}$$

The above in Fourier space.

$$\vec{\mathcal{E}}_F(\vec{r},\omega) = \vec{\mathcal{V}}_F(z,\omega-\omega_0) \tag{3.8}$$

The Helmholtz equation 3.5 reduces within a homogeneus medium in one dimension to

$$\frac{\partial^2}{\partial z^2} \vec{\mathcal{V}}_F(z,\omega-\omega_0) = -\frac{\omega^2}{c^2} n^2(\omega) \vec{\mathcal{V}}_F(z,\omega-\omega_0) \tag{3.9}$$

Using that $\frac{\omega^2}{c^2} n^2(\omega)$ is nothing else but $k^2(\omega)$ the equation becomes

$$\frac{\partial^2}{\partial z^2} \vec{\mathcal{V}}_F(z,\omega-\omega_0) = -k^2(\omega) \vec{\mathcal{V}}_F(z,\omega-\omega_0) \tag{3.10}$$

Which has the trivial solution:

$$\vec{\mathcal{V}}_F(z,\omega-\omega_0) = \vec{\mathcal{U}}_1(\omega-\omega_0) \exp(ik(\omega)z) + \vec{\mathcal{U}}_2(\omega-\omega_0) \exp(-ik(\omega)z) \tag{3.11}$$

We are now choosing only the forward traveling waves, therefore $\vec{\mathcal{U}}_1(\omega-\omega_0) = 0$

$$\vec{\mathcal{V}}_F(z,\omega-\omega_0) = \vec{\mathcal{U}}(\omega-\omega_0) \exp(-ik(\omega)z) \tag{3.12}$$

Therefore the only effect of propagation is in this case the omega dependent phase, generated by the exponential. Lets now introduce a co-propagating frame in fourier space. This is achieved by multiplying the envelope equation with $exp(ik_0 z)$, as for the case of

$k(\omega) = k(\omega_0)$ the exponenital will vanish. The textbook way would be to introduce a transformed time $t' = t - \frac{z}{v_g}$, where v_g is the group velocity, into equation 3.7 anyhow the path chosen here is the more general one. The transformed time directly drops out if equation 3.12 is transformed back into time space. The only thing that needs to be done is to taylor expand $k(\omega) - k_0$ around ω_0 and use the properties of the fourier transform. Anyhow the transformed envelope function will propagate in space.

$$\vec{\mathcal{E}}_F(\vec{r}, \omega) = \vec{\mathcal{V}}_F(z, \omega - \omega_0)\, exp(ik_0 z) \tag{3.13}$$

Plugging 3.12 into the above

$$\vec{\mathcal{V}}_F(z, \omega - \omega_0) = \vec{\mathcal{U}}(\omega - \omega_0) \exp\left(-i\left[k(\omega) - k_0\right] z\right) \tag{3.14}$$

Gives us a simple equation for the envelope propagation for the fundamental.
For the calculation of the propagation of the harmonics, the presence of a polarization term has to be considered. Mathematically we have to solve equation 3.6 instead of 3.5. Which leaves us in the one dimensional case with

$$\frac{\partial^2}{\partial z^2}\vec{\mathcal{E}}_q(z, \omega - \omega_0) = -\left[\frac{\omega^2}{\epsilon_0 c^2}\vec{\mathcal{P}}_q^{NL}(\vec{\mathcal{E}}_F) + k\vec{\mathcal{E}}_q(z, \omega - \omega_0)\right] \tag{3.15}$$

This equation can be solved numerically with an Euler method, meaning that we use the value of $\vec{\mathcal{E}}_q(z, \omega)$ to calculate $\vec{\mathcal{E}}_q(z + \Delta z, \omega)$. This implies that the whole problem can be solved once the initial field $\vec{\mathcal{E}}_q(0, \omega)$ is known. Typically the initial conditions are such that $\vec{\mathcal{E}}_q(\vec{0}, \omega)$ is 0. Therefore the solution path is to start with calculating $\vec{\mathcal{E}}_F$ independently. Then we can obtain $\vec{\mathcal{P}}_q^{NL}(\vec{\mathcal{E}}_F)$ and from there calculate $\vec{\mathcal{E}}_q(z, \omega)$.
The same steps and approximations that have been used here, will be applied later on to extend this principle to the propagation in a waveguide. Anyhow before doing that a more detailed discussion of the motivation of these kind of considerations is in place.

3.2 The Necessity of Phase Matching

Phase matching is a well known phenomenon for all sorts of optical processes involving continuous coherent addition of light waves. It can be visualized by a continuous addition of phasors in a complex plane. Each to be added wave phasors has defined length representing the field amplitude and a defined angle relative to the previous phasor representing the phase. The total length of the resulting sum of phasors gives then the field amplitude of the coherent addition.
In high harmonic generation one of the objectives is to create those harmonics with the highest possible efficiency. Therefore phase matching plays a considerable role. We will discuss several aspects of free space phase matching here based on the assumption that the nonlinear polarization of the q-th harmonic is proportional to $\vec{\mathcal{E}}_F^q$.

$$\vec{\mathcal{P}}_q^{NL} \propto \vec{\mathcal{U}}_F^q(\omega - \omega_0) \exp\left(-iqk_F z\right) \tag{3.16}$$

Plugging the above into equation 3.15 one sees that a coherent addition of polarization and electric field can only be achieved for all z if:

$$\Delta\phi = z\Delta k = z(k_q - qk_F) = m2\pi \tag{3.17}$$

Where m is initially an arbitrary integer. However its clear that this is only fulfilled for

$$\Delta k = k_q - qk_F = 0 \tag{3.18}$$

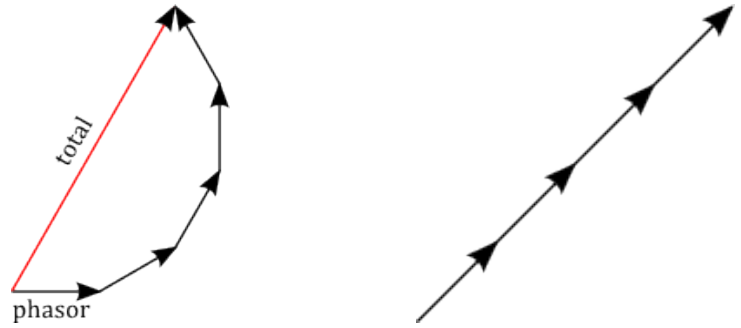

(a) constant phase difference

(b) $n2\pi$ phase difference

Figure 3.1: Coherent addition of phasors of constant length. To the left addition of phasors with constant phase towards each other. To the right addition of phasors with $n2\pi$ phase difference. Clearly the resulting total field amplitude is higher in the right case.

3.2.1 Neutral gas dispersion

The first mechanism that comes to mind is the different wave numbers due to different refractive indices of the medium at different wavelengths. So we find that

$$\Delta k_N = k_q^{vac} n_q - q k_F^{vac} n_F = q k_F^{vac} (n_q - n_F); \tag{3.19}$$

Knowing that the refractive index is just $n = \sqrt{1 + \chi^{(1)}}$ and realizing that $1 \gg \chi^{(1)}$ for the common gases for high harmonic generation. We can Taylor expand n to first order in χ to find

$$\Delta k_N = q k_F \frac{1}{2} \left(\chi_q^{(1)} - \chi_F^{(1)} \right) \tag{3.20}$$

Anyhow we have to keep in mind that we are talking about a macroscopic dielectric susceptibility. Therefore it directly contains the particle density.

$$P = \epsilon_0 \chi^{(1)} E = \epsilon_0 \rho \hat{\chi}^{(1)} E \tag{3.21}$$

Where the particle density ρ is directly related to the pressure of the gas. Assuming that the refractive indices are measured at atmospheric pressure we obtain

$$\Delta k_N = q k_F \frac{P}{P_{atm}} (n_q - n_F) \tag{3.22}$$

The expression can be found in the common literature (for instance [33]) anyhow it additionally contains the change in neutral atom density due to ionization.

$$\Delta k_N = q k_F \frac{P}{P_{atm}} (1 - \eta) (n_q - n_F) \tag{3.23}$$

The parameter η denotes the ionization fraction. For a simple Lorentz model (see next section) one would assume, that $n_q - 1 \gg n_F - 1$ as far off the resonances $n - 1 \propto \frac{1}{\omega_0^2 - \omega^2}$. Therefore *the sign of Δk_N is negative in the case of high order harmonics.*

3.2.2 Free electron dispersion

On an atomic level we can think of the polarization directly as the displacement of an electron off its equilibrium position.

$$P = \epsilon_0 \chi^{(1)} E = N x(\omega) e \tag{3.24}$$

Where N is the density of free electrons. Now we have to find $x(\omega)$. The easiest possible way to do that is thinking of the electron as if initially being in a equilibrium position around the atom. Thinking completely classical we perturb the electron with an external electric field and assume it moving in a quadratic potential, where the spring constant is given by the second derivative of the coulomb potential in space.

$$-\omega^2 x + i\omega\frac{\gamma}{m}x + \frac{k}{m}x = \frac{e}{m}\mathcal{E}(\omega) \tag{3.25}$$

Which has the trivial solution

$$x(\omega) = \frac{e}{m}\mathcal{E}(\omega)\left(\frac{k}{m} + i\omega\frac{\gamma}{m} - \omega^2\right)^{-1} \tag{3.26}$$

From equation 3.24 the expression for $\chi^{(1)}$ directly follows as

$$\chi^{(1)} = N\frac{e^2}{2m\epsilon_0}\left(\frac{k}{m} + i\omega\frac{\gamma}{m} - \omega^2\right)^{-1} \tag{3.27}$$

If $\omega \gg \frac{k}{m}$ we find that

$$n = 1 - N\frac{e^2}{2m\epsilon_0}\frac{1}{\omega^2} \tag{3.28}$$

The difference in wavenumber is then calculated analogously to the neutral atom case as.

$$\Delta k_e = qk_F(n_q - n_F) = qk_F N\frac{e^2}{2m\epsilon_0}\left(\frac{1}{\omega_F^2} - \frac{1}{\omega_q^2}\right) \tag{3.29}$$

Introducing the particle density as function of pressure and the ionization ratio $N = \eta N_{atm}\frac{P}{P_{atm}}$, where N_{atm} is the particle density at atmospheric pressure.

$$\Delta k_e = \eta N_{atm}\frac{P}{P_{atm}}\frac{e^2}{2m\epsilon_0}\frac{k_F}{\omega_F^2}\left(\frac{q^2-1}{q}\right) \tag{3.30}$$

Therefore *the free electron dispersion has a positive sign.*

3.2.3 Properties of the Gaussian beam with regard to phase matching

Due to the generation of most laser radiation in a resonator, laser beams are often well described with a Gaussian beam. When doing HHG in free focusing geometries that implies that there are most of the time Gaussian beams driving the harmonic generation. This section will be devoted to discuss some of their properties with regard to phase matching. The envelope function of an electric field of a linearly polarized Gaussian beam is given by [35]

$$U(r,z) = U_0\frac{w_0}{w(z)}\exp\left(\frac{-r^2}{w^2(z)}\right)\exp\left(-jkz - jk\frac{r^2}{2R(z)} + j\xi(z)\right) \tag{3.31}$$

Where w(z) is the beam waist function, R(z) the wave curvature and $\xi(z)$ is the term representing the Gouy phase. Lets first consider the axial case for $r = 0$ as illustrative case to describe the effects of the Gouy phase.

$$U(0,z) = U_0\frac{w_0}{w(z)}\exp\left(-jkz + j\xi(z)\right) \tag{3.32}$$

Qualitatively the Gouy phase is a phase shift $\Delta\phi = \pi$ for the on axis phase from $z = -\infty$ to $+\infty$, centered around the focus position (see figure fig:gouyphase). Mathematically its given by an arctangent function.

$$\xi(z) = arctan\left(\frac{z}{z_0}\right) \tag{3.33}$$

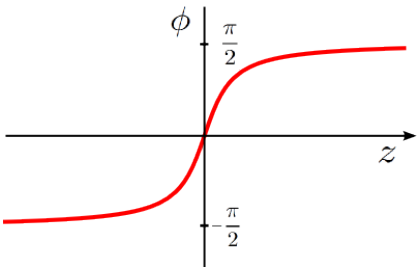

Figure 3.2: A schematic picture of the Gouy phase shift. The focal position is the origin.

With z_0 representing the Rayleigh length. The only thing that we can do here without going into too much detail is looking into the area around the focus. Therefore we can Taylor expand ξ_z around $z = 0$. It follows

$$\hat{k} = k - \frac{1}{z_0} \tag{3.34}$$

Assuming that the harmonic is also Gaussian and that the focal positions agree

$$\Delta k = \hat{k}_q - q\hat{k}_F = k_q - qk_F - \frac{1}{z_q} + q\frac{1}{z_F} \tag{3.35}$$

Further assuming that the Harmonic $E_q \propto E_F^q$ and looking at equation 3.31 we expect that $w_q^2 = \frac{w_0^2}{q}$. Using the definition of the Rayleigh length $z = \frac{w^2\pi}{\lambda}$ [35] we get

$$\Delta k = k_q - qk_F - \frac{\lambda_q}{w_q^2\pi} + q\frac{\lambda_F}{w_F^2\pi} = k_q - qk_F + (q-1)\frac{\lambda_F}{w_F^2\pi} \tag{3.36}$$

For large q, the minus one term in the parenthesis can be neglected, which gives us additional to the neutral gas dispersion and the free electron dispersion a *positive phase contribution* around the focus.

$$\Delta k_G = q\frac{\lambda_F}{w_F^2\pi} \tag{3.37}$$

From a practical point of View this phase contribution has a very unpleasant property. The phase change is biggest where the slope of $\xi(z)$ is biggest, which happens to be exactly at the focus. It is right there where the intensity is highest and we would expect to get the most effective generation of high harmonics. Experimentally this problem is often circumvented by positioning the gas slightly out of the focus and settling with lower intensities in exchange for bigger phase matching volumes. Another rather inconvenient property is the second additional term in the exponential of equation 3.31. Doing the same kind of Taylor expansion in z for this term makes it obvious that it adds a radially depending phase shift. That means that it is already at this point impossible to phase match for instance the whole spot size at once. The limitations above are the sole motivation of switching to a wave guided geometry, as it promises longer interaction regions while not inherently introducing a radial dependent phase shift. The next sections of this chapter will deal with the question if and to what extend that is theoretically possible.

3.2.4 The dipole phase

In the end of chapter 2 it was shown that the atomic phase increases almost linearly with the intensity. However, already there it was pointed out, that this phase is not the relative phase to the electromagnetic field, but the absolute phase gain. Therefore what needs to be done to obtain the actual dipole phase with regard to the q-th harmonic is, strictly thinking classically, to calculate:

$$\Delta\phi = q\omega_0\tau - \phi_{atomic} \tag{3.38}$$

Where ϕ_{atomic} is defined in equation 2.50. This is the phase gain of the harmonic during the propagation in the continuum minus the phase gain of the atomic phase. The problem here is that this is a very ill definition thinking back on the discussion of chapter 2, where we found that ϕ_{atomic} inherently contains contributions from different traveling times τ. This problem can be circumvented using a saddle point approximation in τ. It can then be shown that there are dominant contributions from different τ_{SP} [5], that we will denote as τ_n. It turns out that there are two dominant saddle points, corresponding to two distinct emission times. In literature the trajectories attributed to those emission times are referred to as long and short trajectories. This is due to the fact, that when doing the classical calculations these times correspond to trajectories with significantly different travel times.

Although equation 3.38 is well defined again, there is now a small problem: when having done the calculations in chapter 2, we calculated something like the sum of the two contributions when calculating dipole strength and atomic phase by integrating about all τ. So a different atomic phase for both pathways is expected.

$$\Delta\phi_n = q\omega_0\tau_n - \phi_{atomic,n} \tag{3.39}$$

However, one can show that, treating the integration in τ in equation 2.49 as saddle point approximation [5] yields similar results to equation 2.50 with regard to the linearity of the atomic phase, so that we can write:

$$\Delta\phi_n \propto -\alpha_n I_{light} \tag{3.40}$$

Thereby the radiation corresponding to different saddle points have different dipole phases and thus the phase matching for those contributions differ. A very detailed discussion of this, in a generalized manner, can be found in reference [20].

The next step is to realize that when dealing with laser pulses, there is a temporal dependency on I. For example thinking of a Gaussian laser pulse, the intensity depends on $\exp(-t^2)$.

$$I_{Gauss} = I_0 \exp\left(2\frac{t^2}{\tau^2}\right) \tag{3.41}$$

Therefore, we can relate the position in space to time with the given velocity.

$$\Delta\phi_n \propto -\alpha_n I_0 \exp\left(\frac{x^2}{\gamma^2}\right) \tag{3.42}$$

Now depending on where in space the above expression is Taylor expanded different Δk_{dipole} values are obtained, as k is defined as $k = \frac{\partial}{\partial x}\phi$. In almost any case the Δk_{dipole} value depends linearly on I_0, anyhow it is interesting to point out, that if we Taylor expand $\Delta\phi_n$ around the maximum of the Gaussian, Δk_{dipole} will vanish.anded different Δk_{dipole} values are obtained, as k is defined as $k = \frac{\partial}{\partial x}\phi$. In almost any case the Δk_{dipole} value depends linearly on I_0, anyhow it is interesting to point out, that if we Taylor expand $\Delta\phi_n$ around the maximum of the Gaussian, Δk_{dipole} will vanish.

3.2.5 Experimental parameters for phase matching

Collecting all the Δk terms obtained for the various contributions the resulting total phase mismatch is a function of the gas type, the pressure, the ionization ratio, the order of the harmonic, the focusing conditions and the intensity in the focus. Where the ionization ratio is a function of the intensity as well as the intensity is a function of the focusing conditions. For a given gas type the total Δk is given as follows:

$$\Delta k_{total} = \Delta k_N \left(q, \lambda_F, P, \eta)\right) + \Delta k_e \left(q, \lambda_F, P, \eta\right) + \Delta k_G \left(q, \lambda_f, w_F^2\right) + \Delta k_{dipole} \left(q, I\right) \quad (3.43)$$

The goal is to fulfill the phasematching condition 3.18 for a given harmonic. Equation 3.43 should now point out two things. First the major experimental knobs to turn are the chosen intensity, the gas pressure and the focusing conditions. Anyhow the latter, in particular the Gouy phase causes some trouble. Therefore the ideal geometry would allow a constant intensity distribution over long distances while having a well defined pressure and would circumvent the focusing problem. And second the dependence on the intensity is fairly complicated due to the highly nonlinear dependence of η on I. Δk_N and Δk_e are both linear in pressure and have different prefactors. Therefore up to a certain degree we can control the phasematching by adjusting the pressure. The tunability of the phase matching by pressure changes is anyhow limited, as the refractive index itself itself scales with P. This also counts for its complex part that is responsible for the absorption of the harmonic in the medium. Therefore another experimental knob would be convenient which does not come with this limitation.
We will see later on in this text that using a waveguide geometry offers certain advantages compared to the above. Before this can be discussed a quick introduction to the theory of waveguide propagation is required.

3.3 The Solutions to the Waveguide Geometry

3.3.1 Introduction to propagating fields

Radiation emanating from a laser is usually described by a Gaussian beam. This is due to the fact that this particular basis always solves the Maxwell equations within the boundary conditions constituted by a resonant cavity. Now in oder to understand the propagation in the waveguide geometry we have to find a similar set of basis functions. The starting point here are the free space Maxwell equations for linear polarization. In particular we need the following three relations:

$$\nabla \times \vec{E} = -\frac{d}{dt}\mu_0 \vec{H} \quad (3.44)$$

$$\nabla \times \vec{H} = \frac{d}{dt}\vec{D} \quad (3.45)$$

$$\vec{D} = \epsilon_0 \vec{E} + \vec{P} \quad (3.46)$$

Now restricting us to linear polarization meaning that we need to truncate the time space polarization expansion in first order.

$$\vec{P} = \epsilon_0 \left[\chi^{(1)} \otimes \vec{E} + \left(\chi^{(2)} \otimes \vec{E}\right) \otimes \vec{E} + (\ldots)\right] \quad (3.47)$$

Where $\otimes$ denotes a convolution. Further assuming that we are *dealing with a a single frequency* or a spectral distribution shaped like a delta function $\vec{E} = \vec{E'}\delta(\omega - \omega_0)$ we have a simple time space representation for the polarization.

$$\vec{P} = \epsilon_0 \chi^{(1)} \vec{E} \tag{3.48}$$

Combining the above we end up with two equations that describe the time evolution of all possible electric fields. The first one is equation 3.44 the second is equation 3.49.

$$\nabla \times \vec{H} = \epsilon_0 n^2 \frac{d}{dt} \vec{E} \tag{3.49}$$

Where we have used $n^2 = 1 + \chi^{(1)}$, due to the delta function shaped frequency distribution. To illustrate the procedure lets consider the free space case, meaning no boundary conditions have to be fulfilled. Combining the Grassmann identity $\nabla \times \nabla \times \vec{E} = \nabla \left(\nabla \cdot \vec{E} \right) - \nabla^2 \vec{E}$ with equations 3.44 and 3.49 and using that $\nabla \cdot \vec{E} = 0$ we obtain the Helmholtz equation.

$$\nabla^2 \vec{E} - \frac{1}{c^2} n^2 \frac{d^2}{dt^2} \vec{E} = 0 \tag{3.50}$$

Without boundary conditions to be fulfilled the easiest solution to this equation are plane waves of the form $\vec{E}(x, y, z) = K \vec{e} \exp(i\omega t - ikz)$ where K is some scalar constant. As these plane waves extend to infinity in the x-y-plane they are bound to be unphysical as soon as we are imposing any boundary condition on that plane. This justifies why different solutions are required for different geometries.

3.3.2 Solutions to the cylindrical symmetry

Within this thesis the properties of high harmonic generation within a hollow core waveguide are to be investigated. A hollow core waveguide is one of the simplest possible waveguide geometry representing a glass fiber with an air cylinder in its center. Therefore the boundary conditions that have to be imposed are the ones of a hollow cylinder with a dielectric rim. Due to the symmetry of the problem it is convenient to choose cylindrical coordinates for this discussion. The origin along the radial direction lies then in the center of the inner circle and the z coordinate lies along the axis of rotational symmetry. We choose the boundary between inner and outer material to be at $r = a$. Figure 3.3 schematically depict the choice described above.

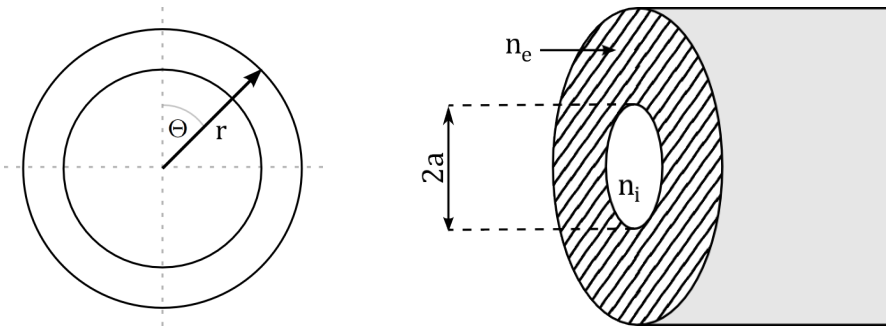

(a) Choice of coordinates (b) Geometry

Figure 3.3: To the left, the chosen cylindrical coordinate system with z pointing into the plane of drawing. To the right a sketch of the fiber geometry with the boundary at $r = a$.

To see how to implement the boundary conditions now its convenient to rewrite equations 3.44 and 3.49 using a more explicit vectorial notation.

$$\begin{pmatrix} \frac{1}{r}\partial_\Theta E_z - \partial_z E_\Theta \\ \partial_z E_r - \partial_r E_z \\ \frac{1}{r}\left(\partial_r (r E_\Theta)\right) - \partial_\Theta E_r \end{pmatrix} = -\mu_0 \begin{pmatrix} \partial_t H_r \\ \partial_t H_\Theta \\ \partial_t H_z \end{pmatrix} \tag{3.51}$$

$$\begin{pmatrix} \frac{1}{r}\partial_\Theta H_z - \partial_z H_\Theta \\ \partial_z H_r - \partial_r H_z \\ \frac{1}{r}\left(\partial_r (r H_\Theta)\right) - \partial_\Theta H_r \end{pmatrix} = \epsilon_0 n^2(r,\Theta,z) \begin{pmatrix} \partial_t E_r \\ \partial_t E_\Theta \\ \partial_t E_z \end{pmatrix} \tag{3.52}$$

Where we have made use of the definition of ∇ in cylindrical coordinates leading to $\nabla \times A = (\frac{1}{r}\partial_\Theta A_z - \partial_z A_\Theta)\vec{e}_r + (\partial_z A_r - \partial_r A_z)\vec{e}_\Theta + \left(\frac{1}{r}\left(\partial_r (r A_\Theta)\right) - \partial_\Theta A_r\right)\vec{e}_z$. If now n is only a function of ω, the solutions $\vec{E}$ to the Helmholtz equation (eq. 3.50) is separable into a transversal solution times an exponential involving time and z. It can further be shown that the same is true for $\vec{H}$ [27]

$$\vec{E}(r,\Theta,z,\omega) = \vec{A}(r,\Theta,\omega)\exp(i\omega t - i\beta(\omega)z) \tag{3.53}$$

$$\vec{H}(r,\Theta,z,\omega) = \vec{G}(r,\Theta,\omega)\exp(i\omega t - i\beta(\omega)z) \tag{3.54}$$

With those equations and the strong restrictions on n the equation system above can be uncoupled. Two partial differential equations are found.

$$\partial_r^2 A_z + \frac{1}{r}\partial_r A_z + \frac{1}{r^2}\partial_\Theta A_z + \left[k^2 n^2(\omega) - \beta^2(\omega)\right] A_z = 0 \tag{3.55}$$

$$\partial_r^2 G_z + \frac{1}{r}\partial_r G_z + \frac{1}{r^2}\partial_\Theta G_z + \left[k^2 n^2(\omega) - \beta^2(\omega)\right] G_z = 0 \tag{3.56}$$

And four additional equations that only depend on the solutions of the above.

$$A_r = \Gamma\left(\beta\partial_r A_z + \frac{\omega\mu_0}{r}\partial_\Theta G_z\right) \tag{3.57}$$

$$A_\Theta = \Gamma\left(\frac{\beta}{r}\partial_\Theta A_z - \omega\mu_0\partial_r G_z\right) \tag{3.58}$$

$$G_r = \Gamma\left(\beta\partial_r G_z - \frac{\omega\epsilon_0 n^2(r)}{r}\partial_\Theta A_z\right) \tag{3.59}$$

$$G_\Theta = \Gamma\left(\frac{\beta}{r}\partial_\Theta G_z + \omega\epsilon_0 n^2(r)\partial_r A_z\right) \tag{3.60}$$

Where $\Gamma = -\frac{i}{k^2 n^2(\omega) - \beta^2(\omega)}$. As a consequence, if the A_z and G_z are known all other components of $\vec{A}$ and $\vec{G}$ are also known. Our main focus now is thus to solve the partial differential equations above. It is straightforward to show that they are separable again and that the angular part needs to have the form $A\cos(m\Theta + \Phi) + B\sin(m\Theta + \Phi)$.

$$A_z(r,\Theta,\omega) = \hat{A}_z(r,\omega)\cos(m\Theta + \Phi) \tag{3.61}$$

$$G_z(r,\Theta,\omega) = \hat{G}_z(r,\omega)\sin(m\Theta + \Phi) \tag{3.62}$$

Therefore equations 3.55 and 3.56 turn into the differential form of the Bessel equations.

$$\partial_r^2 \hat{A}_z + \frac{1}{r}\partial_r \hat{A}_z + \left[k^2 n^2(\omega) - \beta^2(\omega) - \frac{m^2}{r^2}\right]\hat{A}_z = 0 \tag{3.63}$$

$$\partial_r^2 \hat{G}_z + \frac{1}{r}\partial_r \hat{G}_z + \left[k^2 n^2(\omega) - \beta^2(\omega) - \frac{m^2}{r^2}\right]\hat{G}_z = 0 \tag{3.64}$$

This equation is a second order differential equation, therefore there have to be two linearly independent solutions. For our application two formulations are of importance. The first solution is a linear combination of Bessel functions of first kind and Neumann functions [31].

$$S(r) = c_m J_m(\lambda_1(\omega)r) + d_m N_m(\lambda_1(\omega)r) \tag{3.65}$$

The second equivalent solution is a linear combination of Hankel functions of first and second kind [31].

$$S(r) = p_m H_m^{(1)}(\lambda_2(\omega)r) + q_m H_m^{(2)}(\lambda_2(\omega)r) \tag{3.66}$$

The quantities λ_1 and λ_2 are in this context often referred to as transversal wave numbers.

3.3.3 Boundary conditions and introduction to hybrid modes

There are now three classes of solutions to our problem. The transversal electric modes (TE) and the transversal magnetic modes (TM) are both solutions to special cases: $A_z = 0$ for TE respectively $G_z = 0$ for TM. Both cases are fairly straightforward to calculate but of no concern for us for reasons that will be discussed later (see. 3.4.4). The third kind of solutions is the general case for $A_z \neq 0$ and $G_z \neq 0$ this one is not only of interest but also the most complicated one to calculate. These solutions are called hybrid or EH modes. The following section should give a short sketch of their derivation and properties.
The derivation of modes above assumed that $n(r) = const.$ Therefore we have two separate solutions for the region inside and outside the boundary. These two solutions need to fulfill a set of continuity equations at the interface, but first the general requirements. Within the whole geometry there should be no singularities and the solutions need to decay to zero for $r \gg a$. These requirements are fulfilled by the following choice of solutions. For $r < a$ we take equation 3.65 and by requiring no singularities in the geometry the Neumann functions vanish. For $r > a$ we take the formulation with the Hankel functions as solution where we have set q_m to zero. This ensures a proper behavior at $r \gg a$. The continuity in E_z and H_z will be ensured by prefactors in the expressions and identical angular parts for the internal and external part.

$$A_z^{int}(r,\Theta) = c_m J_m(\frac{u}{a}r)\cos(m\Theta + \Phi) \tag{3.67}$$

$$A_z^{ext}(r,\Theta) = c_m \frac{J_m(u)}{H_m^{(1)}(w)} H_m^{(1)}(\frac{w}{a}r)\cos(m\Theta + \Phi) \tag{3.68}$$

$$G_z^{int}(r,\Theta) = p_m J_m(\frac{u}{a}r)\sin(m\Theta + \Phi) \tag{3.69}$$

$$G_z^{ext}(r,\Theta) = p_m \frac{J_m(u)}{H_m^{(1)}(w)} H_m^{(1)}(\frac{w}{a}r)\sin(m\Theta + \Phi) \tag{3.70}$$

Where the variables u and w are frequency dependent. Although not properly defined yet, it is very illustrative at this point to think of m as some sort of mode parameter and to associate $\frac{u}{a}$ respectively $\frac{w}{a}$ as radial wavenumbers. The physical interpretation is then straight forward. The z components of A_m and G_m, for each particular mode m, have a radial dependence governed by a radial wavenumber, which differs from mode to mode and additionally from the inside and outside region of the waveguide. To obtain the full expressions for $\vec{A(\omega)}$ equations 3.67 to 3.70 just have to be plugged into equations 3.57 to 3.60. The result is a bit space consuming and can be found in the references [28, Chap. 9.15]. Figure 3.4 shows a set of possible modes with the respective Bessel functions, the figure is taken directly from reference [30]. Figure 3.5 shows a reproduction of the polarization map for the EH_{-11} mode [1].

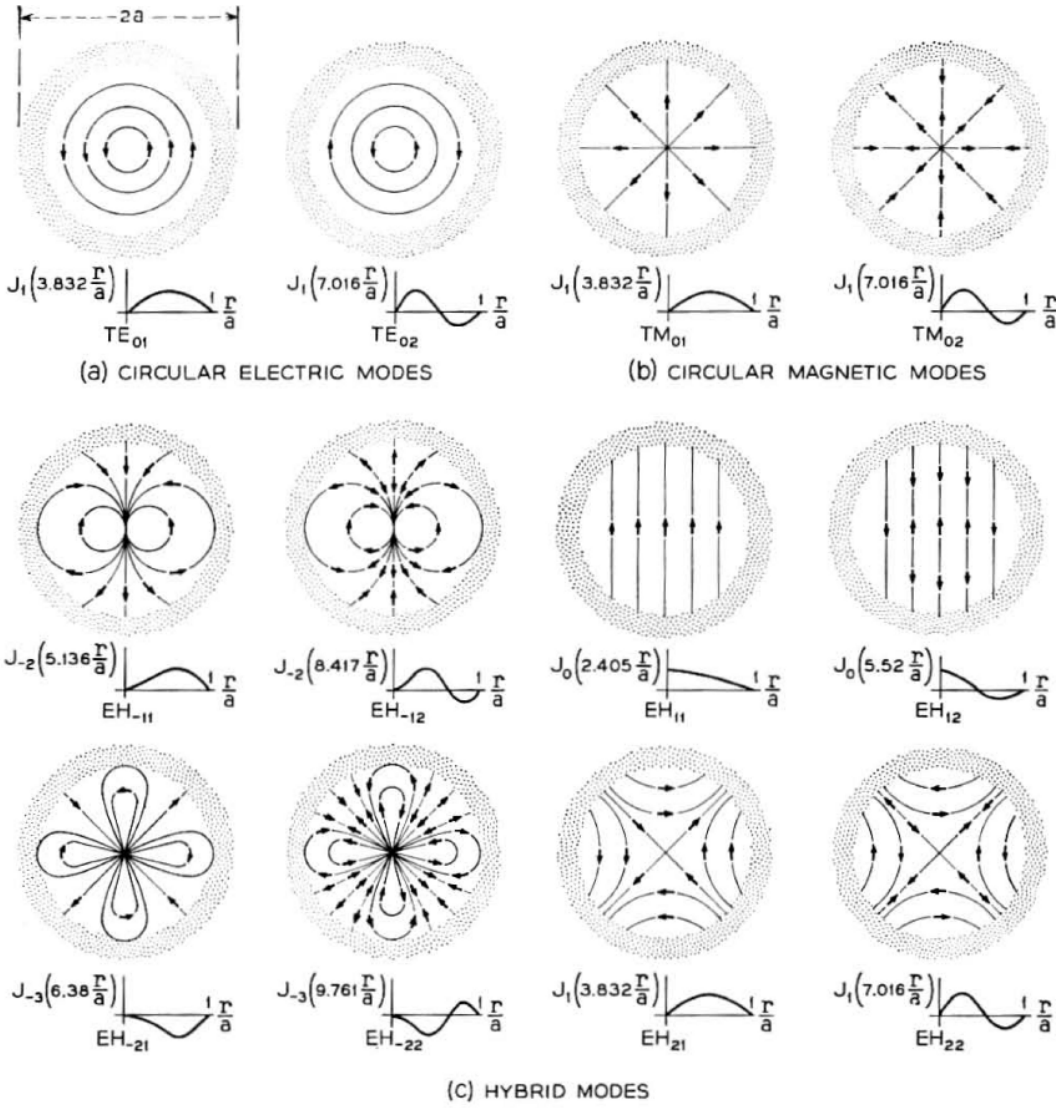

Figure 3.4: Electric field lines and corresponding Bessel functions of modes in hollow dielectric waveguides: (a)transversal electric (b)transversal magnetic and (c)hybrid. Picture taken from reference [30]

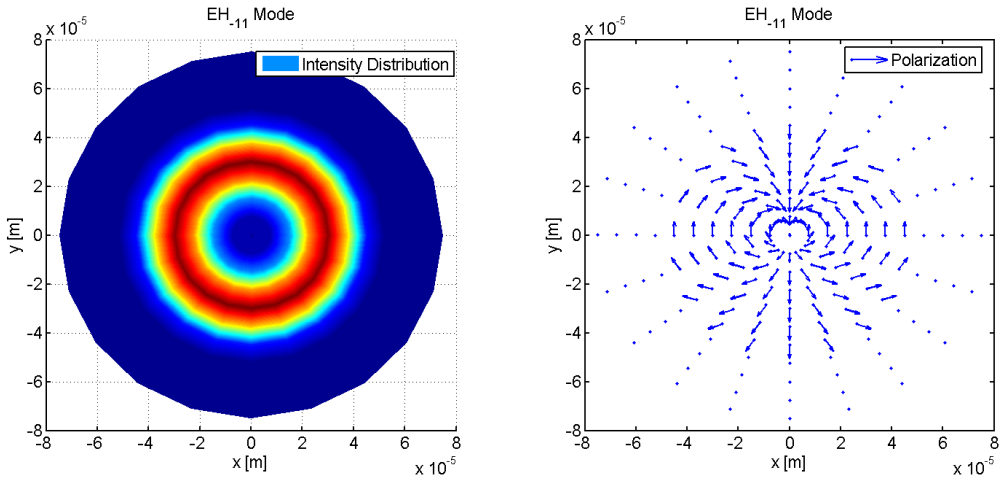

Figure 3.5: Polarization and normalized intensity distribution for the EH_{-11} mode, calculated as described above. General agreement with the sketch from 3.4. The Waveguide radius is in this case $50\mu m$.

There are now four free parameters to be obtained: β, w, u and the relation between c_m and p_m. We will utilize the remaining continuity relations for the boundary at $r = a$ for finding those. From A_Θ we obtain the relation between c_m and p_m.

$$c_m\beta\left(\frac{1}{u^2}-\frac{1}{w^2}\right)m = -p_m\omega\mu_0\left[\frac{J'_m(u)}{uJ_m(u)}-\frac{H'^{(1)}_m(w)}{wH^{(1)}_m(w)}\right] \tag{3.71}$$

The continuity of G_Θ yields equation 3.72.

$$c_m\omega\epsilon_0\left[n_i^2\frac{J'_m(u)}{uJ_m(u)}-n_o^2\frac{H'^{(1)}_m(w)}{wH^{(1)}_m(w)}\right] = -p_m\beta\left(\frac{1}{u^2}-\frac{1}{w^2}\right)m \tag{3.72}$$

Substituting the first continuity equation into the second and eliminating c_m respectively p_m the transcendental dispersion relation is obtained.

$$\left[\frac{J'_m(u)}{J_m(u)}-\frac{u}{w}\frac{H'^{(1)}_m(w)}{H^{(1)}_m(w)}\right]\left[\frac{J'_m(u)}{J_m(u)}-\frac{n_e^2\,u}{n_i^2\,w}\frac{H'^{(1)}_m(w)}{H^{(1)}_m(w)}\right] = \left[\frac{\beta m}{k\,u\,n_i}\right]^2\left[1-\frac{u^2}{w^2}\right]^2 \tag{3.73}$$

3.3.4 Solving the dispersion relation

Although the dispersion relation as given in the previous section can be solved numerically we will use an analytic expression which can be found with certain approximations. First we assume that the radius of the waveguide a is much bigger than the wavelength. Second we restrict ourselves to low loss modes, which are those whose propagation constants β are approximately equal to the free space propagation constant k. Third we assume the refractive index in the center to be one. In this case equation 3.73 can be solved with a perturbation technique [30] yielding a rather simple expression.

$$u(\omega) \approx u_{ml}\left(1 - i\frac{(n_e^2+1)}{\sqrt{n_e^2-1}}\frac{\omega}{ca}\right) \tag{3.74}$$

[1]The nomenclature will be explained in section 3.3.4

Where u_{ml} is the l-th root of the equation 3.75. The usually encountered formulation is $u(k) \approx u_{ml}\left(1 - i\frac{(n_e^2+1)}{\sqrt{n_e^2-1}}\frac{1}{ka}\right)$. This formulation is more convenient as typically one thinks in wavelengths rather than in frequencies.

$$J_{m-1}(u_{ml}) = 0 \tag{3.75}$$

With the relations

$$k_i^2 = n_i^2 k^2 - \beta^2 \tag{3.76}$$
$$k_e^2 = n_e^2 k^2 - \beta^2 \tag{3.77}$$

where $k_i = \frac{u}{a}$ and $k_e = \frac{w}{a}$ are the transversal wave numbers. This explains then the notation used earlier, EH_{ml} refers to the mode with a modeparmeter m and a transversal wavenumber according to the l-th root of J_{m-1}.
We finally have all the parameters we need to fully specify our modes. Inserting the dispersion relation into equation 3.76 and Taylor expanding twice we find the expression for β.

$$\beta_{ml}(\omega) \approx k\left[1 - \frac{1}{2}\left(\frac{u_{ml}\omega}{ca}\right)^2\left(1 - i\frac{(n_e^2+1)}{\sqrt{n_e^2-1}}\frac{2\omega}{ca}\right)\right] \tag{3.78}$$

We see, if we rewrite the above equation in terms of the wavelength that it depends on $(\frac{\lambda}{a})^2$. That means that for $a \gg \lambda$ the axial wavenumber $\beta \to k$. This is the intuitive result we would expect as free space can be interpreted as a special case of a waveguide with infinite diameter. *Anyhow it also allows us to calculate only fundamental as being propagated in modes while calculating the high harmonics in free space. Because with increasing harmonic order the ratio $(\frac{\lambda}{a})^2$ will decrease until almost no mode properties are to be expected.*

$$\beta_{ml}(\lambda) \approx k\left[1 - \frac{1}{2}\left(\frac{u_{ml}}{2\pi}\right)^2\left(\frac{\lambda}{a}\right)^2\left(1 - i\frac{(n_e^2+1)}{\pi\sqrt{n_e^2-1}}\frac{\lambda}{a}\right)\right] \tag{3.79}$$

Now having β_{ml} from the equation above we can calculate u and w. Having u and w, $\vec{A}$ and $\vec{G}$ is fully specified. Anyhow as the only restrictions given for l and m are that they are integer numbers we are dealing with an infinite set of solutions. Keeping in mind, that we solved the problem only for a delta shaped frequency spectrum, the complete solution to the problem is of the shape:

$$\vec{E}(r,\Theta,z,t) = \sum_{ml} c_{ml}\ \vec{A}_{ml}(r,\Theta,\omega)\ \exp(i\omega t - i\ \beta_{ml})(\omega)\ z) \tag{3.80}$$
$$\vec{H}(r,\Theta,z,t) = \sum_{ml} d_{ml}\ \vec{G}_{ml}(r,\Theta,\omega)\ \exp(i\omega t - i\ \beta_{ml}(\omega)\ z) \tag{3.81}$$

Therefore the whole mode propagation problem for a defined wavelength and fiber diameter is solved once the c_{ml} are defined.

3.3.5 Coupling power into the waveguide

The question of how big the individual c_{ml} is again a question of the boundary conditions. We assume that we are at $t = 0$, $z = 0$ and there is a incident field $\vec{E}_{inc}(r,\Theta)$ on the wave guide entrance. The Bessel functions constitute a full basis in two dimensions [31]. That allows us to require

$$\vec{E}_{inc}(r,\Theta) = \sum_{ml} c_{ml}\ \vec{A}_{ml}(r,\Theta,\omega) \tag{3.82}$$

The Bessel functions are by definition orthogonal but not orthonormal. The latter requires us to re normalize the overlap integral so that the c_{ml} are given by

$$c_{ml} = \frac{\int \vec{E}^*_{inc} \cdot \vec{A}_{ml} r\, dr\, d\Theta}{\sqrt{\int \vec{A}^*_{ml}\vec{A}_{ml}\, r\, dr\, d\Theta}} \tag{3.83}$$

We can move the division into the integral, which represents then a normalization of the radial function. From now on *we require the* $\vec{A}^*_{ml}$ *to be normalized* so that $\int \vec{A}^*_{ml}\vec{A}_{ml}\, r\, dr\, d\Theta = 1$. By doing so the c_{ml} just become the scalar product of the two field distributions.

$$c_{ml} = \int \vec{E}^*_{inc}(r,\Theta) \cdot \vec{A}_{ml}(r,\Theta) r\, dr\, d\Theta \tag{3.84}$$

Lets now try to extend this principle to a time dependent electric field. For example a Gaussian laser pulse in space and time is given by

$$\vec{E}(r,\Theta,t) = \vec{E}_0 \exp\left(-\frac{r^2}{\sigma^2}\right) \exp\left(-\frac{t^2}{\tau^2}\right) \exp\left(i\omega_0 t - ikz\right) \tag{3.85}$$

Due to its definition, the envelope function can be separated into a purely scalar time dependence and a radial part.

$$\vec{E}(r,\theta,t) = U(t)\vec{E}_0(r,\Theta) \exp\left(i\omega_0 t - ikz\right) \tag{3.86}$$

Extending equation 3.82 to a time dependent case has a very peculiar problem. As soon as the electrical field contains multiple frequencies we would have to consider individual modes for each frequency and this is exactly the case for the laser pulse described above. The way to circumvent this complication is to assume the mode pattern $\vec{A}_{ml}(r,\Theta,\omega)$ to be approximately $\vec{A}_{ml}(r,\Theta,\omega_0)$ where ω_0 is the center frequency of the impending electrical field. Figure 3.6 shows the dependency of the coupling coefficient of the dominant modes excited by a Gaussian beam. It can be seen, that in the marked area between 100 and 1000 nm there is no significant change visible for the three modes with biggest contained energy. The coupling of the EH_{-11} mode is although exponentially increasing still one order of magnitude smaller than for instance the EH_{13} mode. This justifies the assumption taken above. It has to be pointed out, that the approximations done in the derivations require $1 \gg \frac{\lambda}{a}$, therefore the data for $\frac{\lambda}{a} \geq 0.1$ should be considered as inaccurate.

$$U(t)\vec{E}_0(r,\Theta) \exp\left(i\omega_0 t\right) = \sum_{ml} c_{ml}\ \vec{A}_{ml}(r,\Theta,\omega_0)\ \exp\left(i\omega t\right) \tag{3.87}$$

The final representation is the very simple as every mode will have in this case exactly the same time dependence as the initial pulse had. Which directly implies that the Fourier transform of initial envelope function and mode envelope functions are identical up to a constant factor.

$$c_{ml}(t) = U(t) \int \vec{E}^*_0(r,\Theta) \cdot \vec{A}_{ml}(r,\Theta,\omega_0)\ r\, dr\, d\Theta \tag{3.88}$$

This procedure anyhow only works as long as the time dependence is a purely scalar multiplication. As soon as the incident field changes its radial or angular behavior in time the above does not apply.

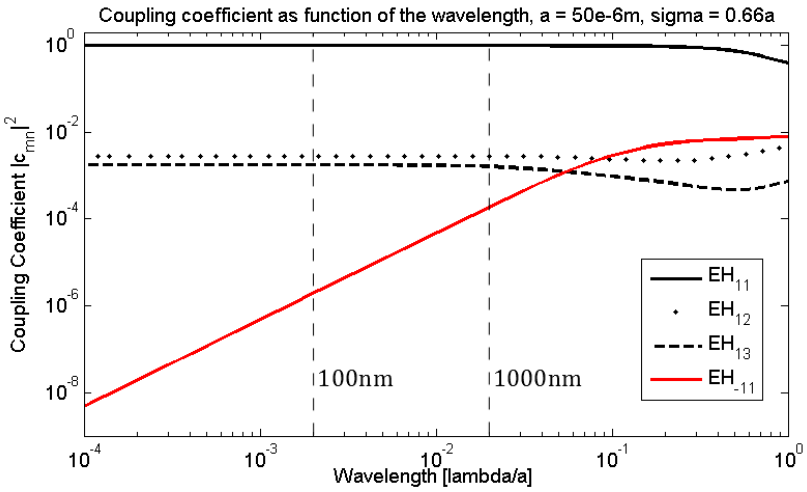

Figure 3.6: Coupling coefficients for an incident Gaussian beam of width σ on a hollow core capillary of radius a = 50e-6m. The Gaussian beam is incident centered on the fiber. The incident field has a normalized power of 1.

3.4 Mode propagation of the Fundamental

3.4.1 The envelope formalism for mode propagation

The goal of the next few pages is to sketch how to obtain a set of scalar equations, describing the mode propagation of the fundamental. From the previous discussion of solutions for the optical waveguide we know that the electric field propagates in modes within the waveguide. The electrical field of a light pulse with a defined envelope can then be written analogously to the free space case as the sum of the modes times a individual scalar envelope function U_n. This was proven in the previous section for a Gaussian pulse but it can be shown in general. [32] Consider a pulse with a center frequency of ω_0:

$$\vec{E}(\vec{r},t) = \sum_n V_n(z,t)\,\vec{A}_n(r,\Theta)\,\exp\left(i\omega_0 t\right) \tag{3.89}$$

Respectively in Fourier space

$$\vec{\mathcal{E}}(\vec{r},\omega) = \sum_n \mathcal{V}_n(z,\omega-\omega_0)\,\vec{A}_n(r,\Theta) \tag{3.90}$$

3.4.2 The envelope equation for mode propagation

In the further discussion of envelope equations, whenever there is a mode distribution $\vec{A}_n(r,\Theta)$, it always refers to $\vec{A}_n(r,\Theta,\omega_0)$. This is possible because we have shown previously that the overlap integrals and therefore indirectly the mode patterns do not significantly change in our region of interest if we allow $\vec{A}$ to be frequency dependent. The idea is now to use the envelope representation of the electric field together with the propagation equation in frequency space for the fundamental (Eq. 3.5). By exploiting the orthonormality of the radial functions (see 3.3.5) $\vec{A}_n(r,\Theta)$ we obtain n scalar equations, where n is the number of modes. For convenience we introduce here a Dirac like notation. So $\vec{A}_n(r,\Theta) = |A_n\rangle$ where we know that $\sum \langle A_m|\ A_n\rangle = \delta(m,n)$. Here $\delta(m,n)$ is the Kronecker function and $\langle A_m|\ A_n\rangle = \iint A_m^*(r,\Theta)\,A_n(r,\Theta)\,r\,dr\,d\Theta$. The result looks already promising, as it resembles closely the Helmholtz equation for the free space case.

$$(\nabla_T^2 + \frac{d^2}{dz^2}) \sum_n \mathcal{V}_n(z, \omega - \omega_0) \, |A_n\rangle + \frac{\omega^2}{c^2} n^2(\omega) \sum_n \mathcal{V}_n(z, \omega - \omega_0) \, |A_n\rangle = 0 \tag{3.91}$$

Where we used the fact that ∇^2 can be decomposed into $(\nabla_T^2 + \frac{d^2}{dz^2})$ a transversal and an axial part. By a projection on $|A_m\rangle$ the principal goal is already achieved, we are left of with n scalar equations describing the propagation of the m-th mode. After some minor algebraic modifications and assuming that $\beta_m(\omega)$ is constant we obtain the final propagation equations 3.92.

$$\sum_n \langle A_m | \, \nabla_T^2 \, |A_n\rangle \, \mathcal{V}_n(z, \omega - \omega_0) + \frac{\partial^2}{\partial z^2} \, \mathcal{V}_n(z, \omega - \omega_0) + \beta_n^2(\omega) \mathcal{V}_n(z, \omega - \omega_0) = 0 \tag{3.92}$$

3.4.3 The paraxial scalar mode propagation equation

A small set of further approximations reduces the mathematical complications required to solve the propagation equations considerably. The first thing to be considered is the transverse gradient matrix element $\langle A_m | \, \nabla_T^2 \, |A_n\rangle$ appearing in the first term of equation 3.92. In general $|A_m\rangle$ would be a function of z, as we know experimentally that there will be plasma formation within the waveguide. It significantly changes the boundary conditions and thereby the solutions to the maxwell equation. Anyhow already by assuming $\beta_m(\omega)$ to be constant *we assume the solutions to be invariant in z.* Therefore within this approximation the transverse gradient matrix element will also be invariant in z.
It turns out that we can completely neglect the first term. Anyhow the argument is a bit more subtle. From the definition of the Matrix element and assuming ∇_T to be for Cartesian coordinates we obtain an integral form.

$$\langle A_m | \, \nabla_T^2 \, |A_n\rangle = \iint A_m^*(x, y) \left(\frac{d^2}{dx^2} + \frac{d^2}{dy^2} \right) A_n(x, y) \, dx \, dy \tag{3.93}$$

Now as the modal field distributions drops to zero at the boundaries of integration, it can be shown that it does not matter which function to differentiate.

$$\int g'(x) \, f(x) \, dx = [f(x) \, g(x)]_{Boundary} - \int g(x) \, f(x) \, dx \tag{3.94}$$

We introduce now $\langle A' | = \nabla_T^2 \, A_m^*(r, \Theta)$. Therefore the transverse gradient matrix element becomes $\langle A'_m | \, A_n \rangle$. Now lets look at the first term of equation 3.92 again and try to find a upper boundary for the expression.

$$\sum_n \langle A'_m | \, A_n \rangle \, \mathcal{U}_n(z, \omega - \omega_0) \tag{3.95}$$

As shown in the next subsection the envelope functions $\mathcal{U}_n$ are related to the fractional power in each mode. Therefore the sum of the squares of the envelope functions can be renormalized to one. Which leaves us with an interesting inequality.

$$\left| \sum_n \langle A'_m | \, A_n \rangle \, \mathcal{U}_n(z, \omega - \omega_0) \right| \leq \left| \sum_n \langle A'_m | \, A_n \rangle \right| \tag{3.96}$$

Now the right hand side in equation 3.96 represents nothing but a projection onto the basis of our normalized mode distributions, which is an unitary operation. Therefore we have proven that the whole expression given above must be smaller than $|\nabla_T^2 \, A_m|$. Therefore *as long as the variation in transversal direction is small compared to the variation of the electric field in axial direction the whole term involving the transverse*

gradient matrix element can be neglected. This is called the paraxial approximation. In our case the variation of the mode pattern is on a characteristic scale of the fiber diameter while the variation in axial direction is on the scale of the wavelength, the approximation seems thereby reasonable. An interesting side effect is that by dropping this term the equation system is also automatically uncoupled, meaning that the evolution of the individual modes is not influenced by each other.
After having applied all of the approximations introduced above the initial set of coupled second order differential equations become a set of independent homogeneous first order differential equations that we have seen already in 3.1.3.

$$\frac{\partial^2}{\partial z^2}\mathcal{V}_n(z,\omega-\omega_0) = -\beta_n^2(\omega)\mathcal{V}_n(z,\omega-\omega_0) \tag{3.97}$$

Which has the solutions:

$$\mathcal{V}_n(z,\omega-\omega_0) = \mathcal{U}_n(\omega-\omega_0)\exp\left(-i\beta_n(\omega)z\right) \tag{3.98}$$

As we would expect the obtained equations converge to the free space envelope equation (Eq. 3.14) for the case of $r \to \infty$ as then $\beta_m(\omega_0) \to k(\omega_0)$ and $\beta_m(\omega) \to k(\omega_0)$. As a final step we introduce the co-propagating frame for each of the modes.

$$\mathcal{V}_n(z,\omega-\omega_0) = \mathcal{U}_n(\omega-\omega_0)\exp\left(-i\left[\beta_n(\omega)-\beta_n(\omega_0)\right]z\right) \tag{3.99}$$

It has already been described how to obtain the $\vec{U}(t)$ (see 3.3.5) for our purpose. The quantity $\vec{\mathcal{U}}_n(\omega-\omega_0)$ occurring here is just the Fourier transform of the initial one shifted to be centered in frequency around zero. We are now left with basically an infinite set of equations that all need to be solved in order to obtain the electric field at each position in space. Anyhow the next section will deal with how to limit the amount of to be considered modes.

3.4.4 The active mode approximation

In the previous section it was shown that for our conditions the transverse gradient term can be neglected. Therefore there will be no coupling of energy between the individual modes during the propagation (see eq 3.92), as already in the very beginning only linear propagation was assumed. This again means that we have to consider in the propagation only the modes that the incident field on the fiber entrance couples to. Restricting ourselves to the case where the incident field is linearly polarized and Gaussian in space an time, we find that there is only a few modes that actually have to be taken into account. Figure 3.7 displays the mode coupling of a Gaussian beam for different modes for a defined $\frac{\sigma}{a}$.
Repeating these simulations for various values of $\frac{\sigma}{a}$ we find that for a region around $\frac{\sigma}{a} = 0.64$ more than 98% of the power is coupled into the EH_{11} mode. Figure 3.8 shows the simulations on how the focal size of the incident gaussian beam affects the coupling coefficient of the dominant modes. Said figure has two interesting features; it not only shows that for the right focusing conditions almost all power is coupled into a distinct mode, it also shows that for a broad range of $0.3 > \frac{\sigma}{a} > 0.7$ that the first three of the EH_{1m} cover almost 100% of the guided power.
The conclusion here is that it is sufficient in the conditions assumed here, to consider only the EH_{1m} modes and of those also only the lower orders. The conclusion that has been reached above in a purely mathematical way can be qualitatively explained by looking at figure 3.4 and reminding ourselves that by calculating the coupling coefficient we calculate the mode overlap integral between the incident field and the particular mode. The EH_{1m} modes are the only modes that are linearly polarized and therefore show the biggest overlap with our initially linearly polarized Gaussian beam. The active mode approximation is also the reason why we were allowed to neglect the TE and TM modes

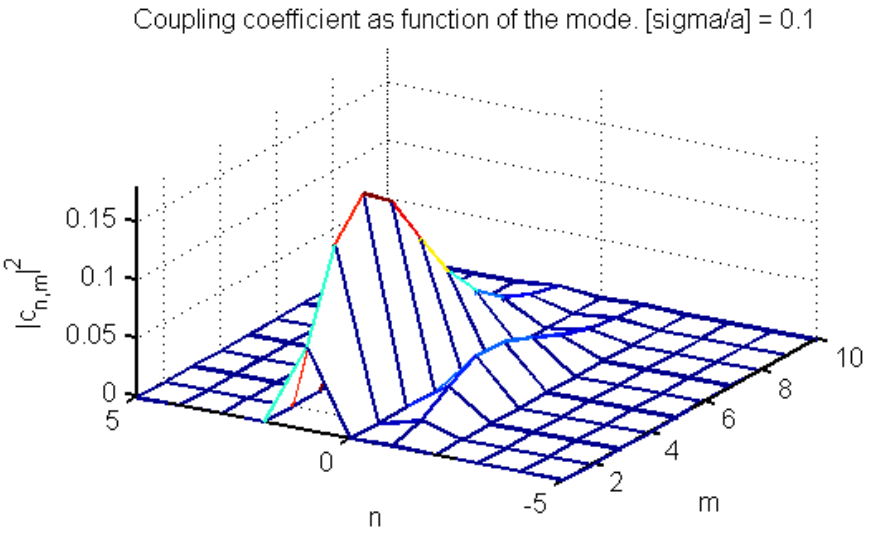

Figure 3.7: Coupling coefficients for a incident Gaussian beam of width σ on a hollow core capillary of radius a = 50e-6m. The Gaussian beam is incident centered on the fiber. For this ratio of $\frac{\sigma}{a}$ there seems to be only coupling into the lower orders of the EH_{1m} and EH_{-1m} modes. The sum of all $|c_{mn}|^2$ displayed here is 0.97, for an electric field with normalized power 1.

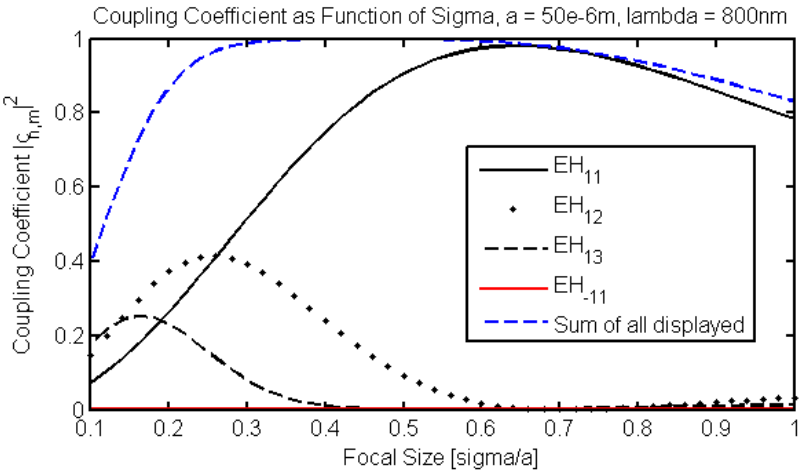

Figure 3.8: Coupling coefficients of the dominant modes of a incident Gaussian beam of width σ on a hollow core capillary of radius a = 50e-6m. The Gaussian beam is incident centered on the fiber. For $\frac{\sigma}{a} = 0.64$ the coupling efficiency is about 98%

.

Mode	Radius	$Re(\beta) - k_{vac}$	$\frac{\partial}{\partial\lambda}\left(Re(\beta) - k_{vac}\right)\vert_{800nm}$	$Im(\beta)$	abs. length
	$[\mu m]$	$[\frac{1}{m}]$		$[\frac{1}{m}]$	$[cm]$
EH_{11}	90	-45	-0.057	0.194	515
	130	-22	-0.028	0.065	1538
	150	-16	-0.021	0.042	2381
EH_{12}	90	-239	-0.30	1.024	98
	130	-115	-0.15	0.340	294
	150	-86	-0.11	0.221	452
EH_{13}	90	-589	-0.75	2.516	38
	130	-282	-0.35	0.835	120
	150	-212	-0.27	0.543	184

Table 3.1: Collection of propagation properties for the three to be used fiber radii at 800nm. The parameter $Re(\beta) - k_{vac}$ gives the variation of the axial wavenumber due to the presence of the guiding structure. $\frac{\partial}{\partial\lambda}\left(Re(\beta) - k_{vac}\right)\vert_{800nm}$ gives a measure for the introduced dispersion. $Im(\beta)$ and the absorption length are both a measure of the absorption intuced by the waveguide. The absorption length is her defined as the length where the power drops by a factor of e^{-1}.

completely in our discussion. It can be shown analytically that the overlap integral between our linearly polarized Gaussian and the TE respectively TM modes is always zero.

3.4.5 Dispersion properties of the dominant modes

Although the dispersion properties are basically all given by the dispersion relation (Eq. 3.79) it is instructive to discuss its properties for the dominant modes. For convenience we shall restate the dispersion relation:

$$\beta_{ml}(\lambda) \approx k\left[1 - \frac{1}{2}\left(\frac{u_{ml}}{2\pi}\right)^2\left(\frac{\lambda}{a}\right)^2\left(1 - i\frac{(n_e^2+1)}{\pi\sqrt{n_e^2-1}}\frac{\lambda}{a}\right)\right]$$

The glass type of the thick wall capillaries used in the experiments is a unspecified Borosilicate glass. Lets assume for now that its optical properties are comparable to those for typical borosilicate glasses like Schott N-BK7. For Schott N-BK7 the manufacturer specifies the refractive index to be about 1.513 at 700nm and 1.509 at 900nm, therefore only changing 0.3% in that range. Looking at the dispersion equation it is reasonable to neglect the wavelength dependence of n and to assume $n_e \approx 1.5$. Figure 3.9 displays now the results of calculations where the waveguide radius a was kept at 50 μm and the wavelength was changed. The general feature is that for higher wavelengths the real part decreases and the imaginary part increases. The higher the order of a mode is the lower its is real part and the higher its absorption is. All of the modes display a lower propagation constant as the free space case. Without doing the same kind of plots for the dependency on a change in radius, the structure of the dispersion equation requires the behaviour to be exactely the other way round. Table 3.1 lists the fiber properties for the different core radii to be used in the experiment.

3.5 Phasematching in Waveguides

The discussion started in 3.2 can now be continued. We left of to discuss the propagation properties of a hollow core waveguide, expecting that the waveguide may have better properties with regard to phase matching than the free focusing geometry has. It has been shown now that the waveguide geometry provides a confinement of the pulse for up to

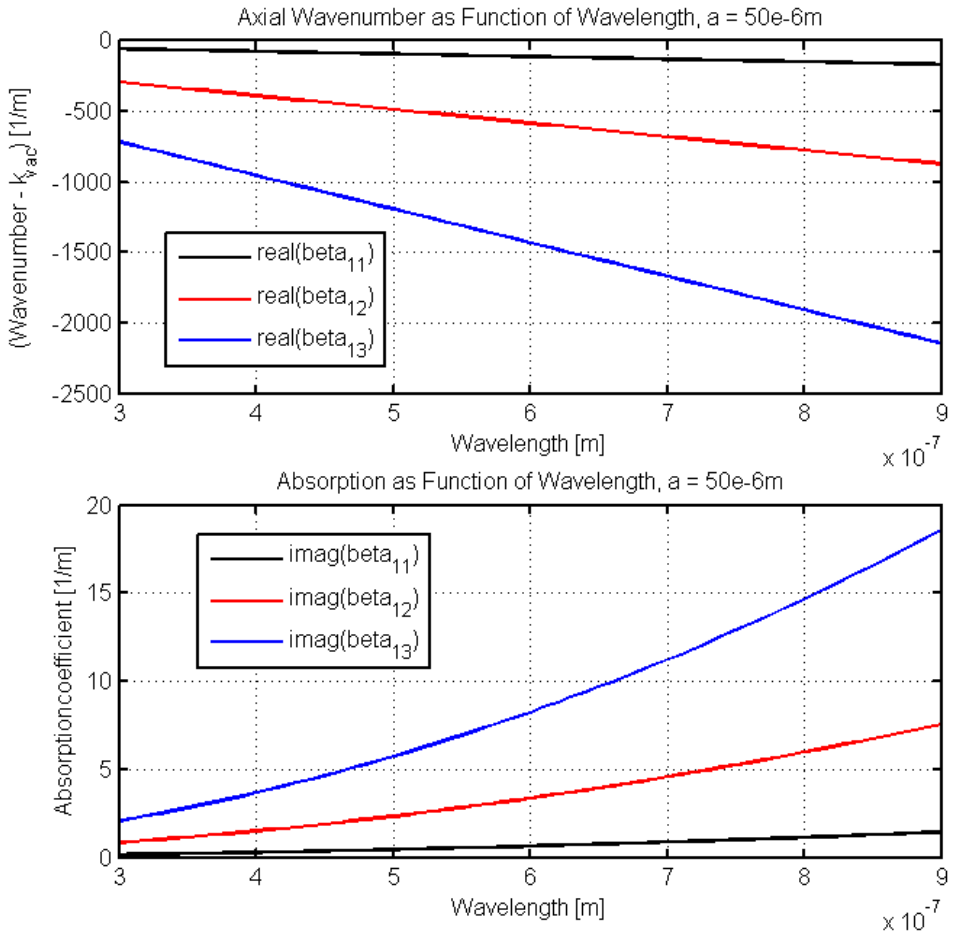

Figure 3.9: Calculations based on the dispersion relation given in the text. Top the real part of β_n as a function of λ and the same thing for the imaginary part of β_n at the bottom. The inner diameter of the waveguide was kept at $50\mu m$.

several meters for individual modes (see table 3.1). Additionally to the confinement there is no radial or angular dependence on the wavenumber. In this section we will try to quantify this behavior a little more. Anyhow, compared to section 3.2 we are bound to the approximations done in the derivation of the propagation equations above. Therefore it has to be assumed that $k(\omega)$ does not change in r or z. If there are significant changes with regard to those parameters the solutions found for the wave guide geometry are no longer valid. Compared to the free parameters used in the free focusing case this means it has to be assumed that there is only minor free electron generation.
Again it will be assumed, that the nonlinear polarization of the q-th harmonic is proportional to $\vec{\mathcal{E}}_F^q$.

$$\vec{P}_q^{NL} \propto \left[\sum_n \mathcal{U}_n(z, \omega - \omega_0)\, \vec{A}_n(r, \Theta) \exp\left(-i\beta_n(\omega) z\right)\right]^q \tag{3.100}$$

3.5.1 The single active mode approximation

This time the resulting polarization is not as easy to handle as in the free focusing case. There are now countless cross terms that combine envelope functions, mode distributions and propagation constants of up to q modes. It is anyhow interesting to discuss a case where simple analytic expressions can be found. For instance lets again take the Gaussian beam with appropriate width impending on a hollow core waveguide. It was shown before that c_{11} is much greater than all other coupling coefficients (see figure 3.8 and 3.6). And therefore $\mathcal{U}_{11}(z, \omega - \omega_0)$ must be much greater than all other envelope functions. The conclusion here is, that for this special case its sufficient to consider

$$\vec{P}_q^{NL} \propto \mathcal{U}_{11}^q(z, \omega - \omega_0)\, \vec{A}_{11}^q(r, \Theta) \exp\left(-iq\beta_{11}(\omega) z\right) \tag{3.101}$$

Figure 3.10 depicts now the intensity profile and the polarization map of the EH_{11} mode. Up to small deviations at the boundaries the polarization is completely linear. This allows us to replace the mode distribution here by a unit vector pointing into the direction of the initial Gaussian.

$$\vec{P}_q^{NL} \propto \mathcal{U}_{11}^q(z, \omega - \omega_0)\, \exp\left(-iq\beta_{11}(\omega) z\right) \hat{e}_{Gauss} \tag{3.102}$$

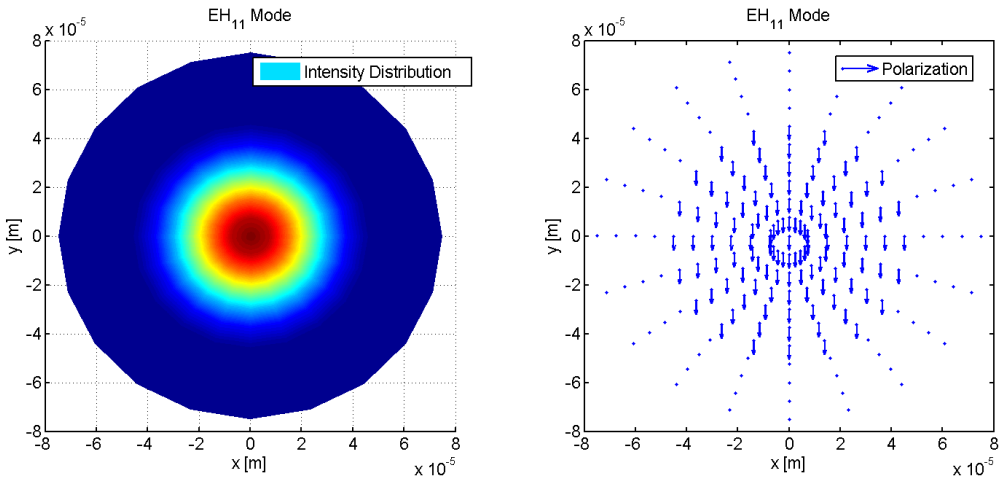

Figure 3.10: Polarization and normalized intensity distribution for the EH_{11} mode. The Waveguide radius is in this case $50\mu m$.

Equation 3.18 then becomes

$$\Delta k = k_q - q\beta_{11} \tag{3.103}$$

3.5.2 Neutral gas dispersion in waveguides

The rest of this section will closely resemble the discussion in section 3.2, just that this time the wave guide geometry is considered. All the quantities introduced there will not be introduced again here, in case of doubt please refer to section 3.2.

The dispersion relation 3.79 can be written in a slightly different form

$$\beta_{ml}(\lambda) \approx k\left[1 - \epsilon_{ml}(\lambda, a)\right] \tag{3.104}$$

In the initial reference [30] it was assumed that the inner refractive index in the waveguide is one, k in the expression above represents then the vacuum wavenumber. Anyhow the inner refractive index can be treated as a perturbation to this case. Therefore we obtain an equation, consistent with the free space derivations.

$$\beta_{ml}(\omega) \approx k_F^{vac} n_F\left[1 - \epsilon_{ml}(\lambda, a)\right] \tag{3.105}$$

This expression has the expected asymptotic behavior for $\frac{a}{\lambda} \to \infty$ respectively $\epsilon \to 0$.

$$\Delta k = q k_F^{vac}\left(n_q - n_F[1 - \epsilon_{ml}]\right) \tag{3.106}$$

which is clearly positive as $n_q > 1$. The rest of the derivation works analogously to the free focusing case and leads to an almost identical expression.

$$\Delta k_N = q k_F \frac{P}{P_{atm}}(1 - \eta)\left(n_q - n_F\left[1 - \epsilon_{ml}\right]\right) \tag{3.107}$$

It follows that for small ϵ_{ml} the sign of Δk_N remains positive for the same reasons as given in 3.2.1.

3.5.3 Free electron dispersion in waveguides

Using equations 3.28 and 3.106 an analogous expression to 3.29 is obtained.

$$\Delta k_e = q k_F N \frac{e^2}{2m\epsilon_0}\left[\frac{1}{\omega_F^2} - \frac{1}{\omega_q^2} - \epsilon_{ml}\left(\frac{2m\epsilon_0}{Ne^2} - \frac{1}{\omega_F^2}\right)\right] \tag{3.108}$$

Which can be rewritten to

$$\Delta k_e = q k_F N \frac{e^2}{2m\epsilon_0}\left[\frac{1 + \epsilon_{ml}}{\omega_F^2} - \frac{1}{\omega_q^2}\right] - \epsilon_{ml} q k_F \tag{3.109}$$

Or in a form similar to 3.30

$$\Delta k_e = q k_F N_{atm} \frac{P}{P_{atm}} \frac{e^2}{2m\epsilon_0\omega_F^2}\left[\frac{(1 + \epsilon_{ml})q^2 - 1}{q}\right] - \epsilon_{ml} q k_F \tag{3.110}$$

As ϵ_{ml} is assumed to be small, Δk_e is still positive.

3.5.4 The dipole phase in waveguides

The discussion of the dipole phase in waveguides is completely analogous to the discussion in the free focusing geometry. This is not surprising, as within the atomic process nothing has changed. Therefore the dipole phase term behaves the same way in both geometries.

3.5.5 Conclusion of the phasematching properties

Collecting all the Δk terms obtained for the various contributions again we find an almost identical relation as before. The only differences are that the Gouy term disappeared and that Δk_N and Δk_e are additionally dependent on the inner diameter of the waveguide.

$$\Delta k_{total}^{waveguide} = \Delta k_N\left(q, \lambda_F, a, P, \eta\right) + \Delta k_e\left(q, \lambda_F, a, P, \eta\right) + \Delta k_{dipole}\left(q, I\right) \tag{3.111}$$

Therewith all the problems pointed out in 3.2.5 have been resolved. First, the phase matching does no longer depend on the focusing conditions while the intensity is conserved over much longer distances than possible in a reasonable free focusing geometry (see table 3.1. Second it seems much more feasible to maintain a defined pressure over such a long distance within a fiber than within free space. Third we found an additional free parameter that can be experimentally tweaked. Anyhow there are some drawbacks. Foremost, the derivation only allows ionization fractions much smaller than one. Also there is still a radial dependence of the phase, caused by the fact that the intensity is a function of the radius. If it was possible to find a fiber geometry that fulfills all the previous requirements that we demanded to get to this point, and additionally provides a dominant Eigen mode with a very low intensity gradient in the center, an almost perfect HHG geometry would have been found. To illustrate this, figure 3.11 shows the radial dependence of the intensity for a Gaussian field distribution and a J_0 field distribution as for the EH_{11} mode. One can imagine more sophisticated fiber geometries with flat top like profiles.

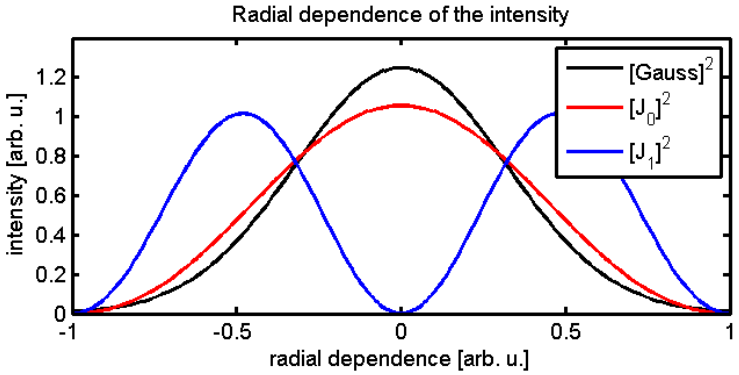

Figure 3.11: Radial dependence of the intensity for a Gaussian, J_0 and J_1 field distribution. All functions are normalized to the same area. The width of the Gaussian is chosen such that $\frac{sigma}{a} = 0.64$, representing the optimal coupling conditions for the EH_{11} mode.

3.6 Conclusion on Chapter 3

In this chapter the mathematical and physical tools required to do simple calculations on high harmonic generation in hollow core capillaries have been introduced, motivated and proven as far as possible. Same goes for the approximations and assumptions done in the process of finding these tools. The solution strategy for the propagation of a simple Gaussian pulse should now be clear. It can be summarized as follows.

1. Calculate propagation of fundamental
    a) find modes
    b) decompose pulse into mode envelope functions
    c) single out the dominant modes
    d) transform envelope functions to frequency space
    e) propagate with envelope equation

2. Calculate propagation of harmonic
    a) get nonlinear polarization from fundamental
    b) propagate with envelope equation
    c) transform result back into time space

Additional to this, analytic considerations on the phase matching condition and coherent buildup of high harmonics were presented. The important points there are, that the possible phase matching volume is considerably higher than everything that can be achieved with a free focusing geometry while getting rid of the Gouy phase contribution. The fundamentally different intensity distributions that can be encountered in this very simple case of a wave guide should hint at possible further application with tailored waveguides to achieve even higher phase matching volumes and conversion efficiencies. Finally, it must be kept in mind that in developing this formalism a couple of strong approximations have been made. The linearization of the propagation equations and the Born approximation (see: 3.1.2) most notably. This example was picked for the reason, that it is known that lower order harmonics contribute significantly to the high order harmonic generation process itself. Anyhow this is beyond the scope of the simple theoretical considerations that the author wanted to present here. It was the goal to maintain as much generality as necessary to motivate the experiment suggested in the next chapter. For more meticulous and general derivations see [37, 36] for short pulse propagation in general and [38, 39] for propagation equations in fibers with present plasma. There are also several classical papers dealing with propagation of high harmonics anyhow using more complicated derivations in time space [13, 14, 16] and in particular [4].

Chapter 4

Experimental Status and Outlook

4.1 Introduction

4.1.1 HHG in gas cells

Today the main source for XUV radiation at the Attosecond Science Group of Lund University is high-order harmonic radiation generated in gas cells. These gas cells are basically cylindrical channels in an Aluminum block connected to a fast piezo valve [40]. Compared to the free focusing geometry described in the introduction, they allow to maintain a controlled gas pressure over a distance of about 1 cm. The channel of such a cell has a diameter of approximately 0.5 mm. A gas cell that has been used for HHG is displayed on figure 4.1.

These gas cells are mounted on a 5 axis translation stage that contains the piezo valve itself and are placed in a vacuum chamber. Gas cell and mounting stage are shown on figure 4.2. The lower energy arm of the Lund High-Power Laser Facility, providing pulses with energies of up to 100 mJ with durations down to 45 fs (FWHM) at a repetition rate of 10 Hz is focused into this gas cells with a focal length of several meters (f = 2-6 m). The long focal lenghts provide a long raleigh lenght, this is required to maintain a high intensity over the extend of the cell. A XUV spectrometer is directly connected to the chamber, allowing to measure the generated harmonics spectrally resolved. The setup as used with the gas cells is described here [42].

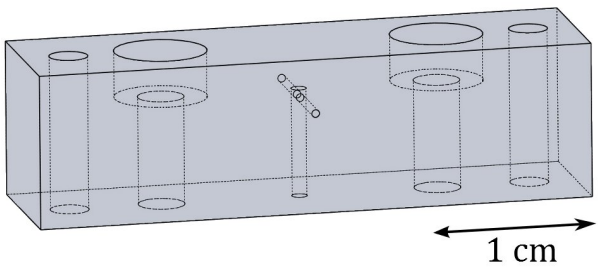

Figure 4.1: Sketch of a gas cell as used in current experiments on HHG. The vertical hole in the center constitutes the connection to the piezo valve while the attached perpendicular channel is the actual gas cell. The intial work related to these cells can be found here [41].

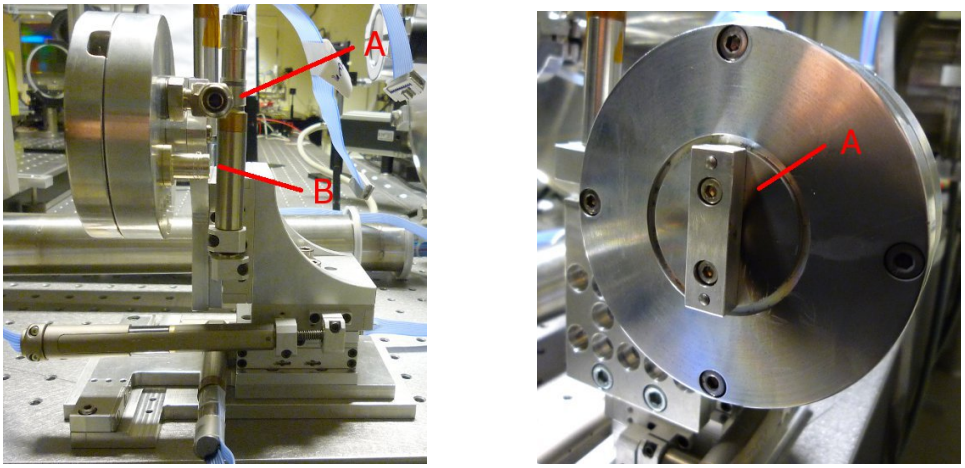

Figure 4.2: On the left: the 5 axis stage with the connected piezo valve. The gas connector (A) and control voltage socket (B) of the valve is clearly visible. To the right: a gas cell (A) connected to the same stage. Here the mounting system can be seen. Two M3 screws plus two bolts keep the cell in place.

4.1.2 The paradigm of the experiment

The initial goal of the work was to compare the HHG performance of gas cells to waveguides in terms of experimental handling and photon yield. The general idea is to start with comparable diameters and lengths of gas cell and waveguide, to gradually decrease the waveguide diameter and length and monitor what happens with the photon yield.

In a first step towards this we will try to measure HHG in waveguides and to compare the phase matching pressures to the ones published by the group of Henry Kapteyn and Margret Murnane at JILA Colorado. For a 23fs pulse with a pulse energy from 125 to 1640 μJ in a 150 μm waveguide filled with Argon they claim a optimal phase matching pressure of between 10 and 60 torr, corresponding to 10 to 70 mbar[33, 34].

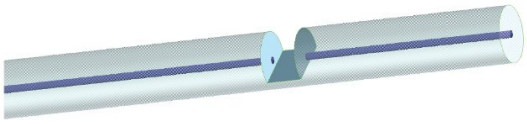

Figure 4.3: Rendering of a slotted inner capillary, as used in a early iteration of the experiments done at JILA. The width of the slot was in their case $\frac{1}{32}$ of an inch or approximately 0.8mm. Picture taken from [34].

For this first stage waveguides were bought with a diameter of 160 μm and prepared in a similar manner as proposed by them. This includes adding two gas inlet slots on both ends of the fiber, what is meant with a gas inlet slot is depicted on figure 4.3. The waveguides where bought from Vitrocom, the company sells them as heavy wall borosilicate capillaries in a broad range of inner and outer diameters. The straightness was guaranteed to be better than 10 μm on 10cm capillary length and the roundness was specified to have less

than 3.5 μm deviation from the circle for a 0.150 μm inner diameter capillary. The slots were added by Scientific Lab Glass Lund AB with a diamond disc saw. Figure 4.4 shows one of our capillaries prepared with the gas inlet slot.

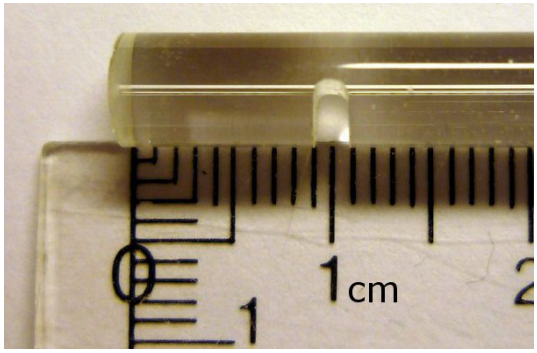

Figure 4.4: Vitrocom HWC010-55 heavy wall capillary with added gas inlet slot. The slot width is about 2 mm.

4.2 Design and Development of the Fiber Mount

Having the fibers, a suitable mount was needed that allowed to deliver the appropriate backing pressure to the gas inlets, while not leaking any unnecessary gas into the vacuum. There were different fairly advanced designs by other groups, most notably the V-groove mount presented in Ariel J. Pauls thesis[34]. However the design presented here deviates significantly from any of those, due to being adapted particularly for our vacuum system and the given manufacturing possibilities.

4.2.1 Development considerations

In order to allow an easy and uncomplicated change between gas cells and waveguides the waveguide mount needed to be compatible with the gas cell mounting system, therefore have the same sort of attachment points as the gas cells have (see figure 4.2). Furthermore, it should be possible to mount and unmount the wave guide system without needing to remove the translation stage from the vacuum chamber. This implies that all the screws that need to be unscrewed for removing the mount should be accessible from the top.

Another feature that was required from the mount was to support variable waveguide lengths and allow variable inlet positions, while at the same time the center piece of the waveguide should be visible from the top in order to support the alignment procedure and to allow direct monitoring of the processes inside. Also for alignment reasons it was necessary, that the waveguide entrance can be located at the same position as the gas cell entrance, as this is the center of rotation for the 5-way gas cell holder. Positions different from that would complicate the alignment procedure significantly.

4.2.2 The design

The design we came up with was then a modification of a mount presented by F. Wojda in his thesis [43]. It relies on two gas delivery end pieces that the waveguide is glued in with a silicone glue.[1] These two end pieces can then be moved relative to each other in a rail,

[1] So far we have not tried to mount the system with an actual waveguide, anyhow the glue that we plan to use will be Loctite AS 310. This type of silicone clue is vacuum compatible and was recommended for this purpose by other groups.

allowing changing inlet positions and waveguide lengths. The end piece design is shown in figure 4.5.

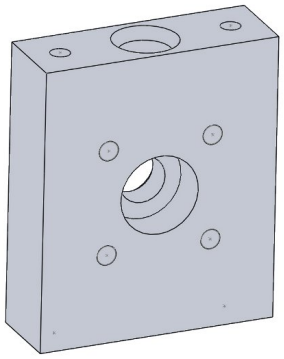

Figure 4.5: The end piece for the waveguide mount. The gas streams in through the top into the volume in the center where the gas inlets of the waveguide are positioned. A lid is screwed on top of the end piece, that allows to seal the volume from both sides with silicone glue.

The easy mounting and un-mounting issue was solved by having a separate mounting plate to which the rail was fixed by two M3 screws. This mounting plate has the screws and bolts layout as the gas cell has and can thus be attached on top of the piezo valve just like the cell. The piezo valve can then be used to control the gas flow into the waveguide. The final mount is presented in figure 4.6. It fulfills all the requirements given. The biggest drawback of our mount will probably be the fairly long time that is required to replace a damaged waveguide or to switch to a different waveguide in an experiment. The alignment will also be lost every time the waveguide is changed. However, it should be noted that breaking and re-establishing the vacuum takes the longest time in the procedure of changing capillaries. This is the same for all possible designs.

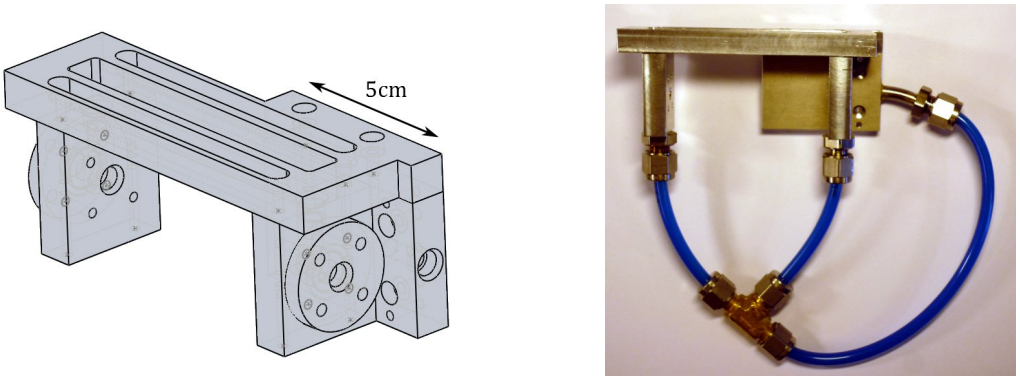

Figure 4.6: On the left: the final design for the capillary holder. The two end pieces can be moved in a rail. The rail itself can be easily unscrewed from the mounting plate in the back. On the right: the assembly with the gas connectors attached. The lids for the end pieces are missing in this picture.

4.3 Calculations on Pressure Dynamics

As it was shown in chapter 3, the pressure distribution plays a significant role in the phase matching for HHG. The choice of a hollow core wave guide can also be justified solely by the possibility of providing a constant gas pressure over almost arbitrary distances. However, there is the technical boundary condition that the current gas supply is built to deliver a pulsed gas jet as described earlier in this chapter. Therefore the system layout is designed for delivering gas flow to a completely different geometry. It needs to be investigated, whether a pulsed backing pressure for the waveguides is feasible in terms of the expected time constants and expected gas flow. The aim of modelling the gas flow is to obtain an order of magnitude estimation of the required parameters for the opening time of the piezo valve and the overall backing pressure.

4.3.1 Modeling of the gas flow

The first step in the process of modeling the gas flow is to ecompose the geometry into a set of volume elements of constant circular cross section at constant pressure.

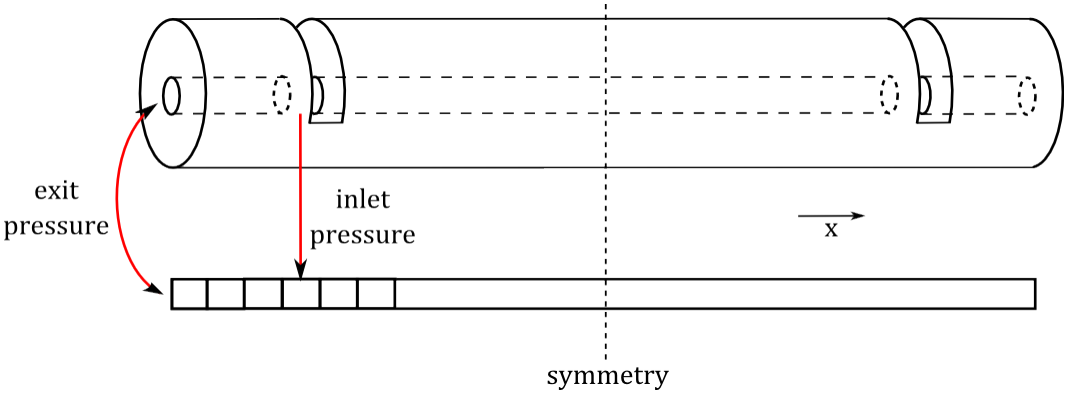

Figure 4.7: 1D waveguide model. Decomposition of the geometry into volume elements of constant circular cross sections at constant pressure.

The gasflow can then be modelled rather easily, if the following assumptions apply:

1. The flow can be considered laminar.
2. The fluid is approximately incompressible.
3. The flow is through a constant circular cross section.
4. The circular cross crossection is significantly longer than its diameter.

The volumetric flow $\Phi = \frac{\partial V}{\partial t} \approx \frac{\Delta V}{\Delta t}$ is given by the Hagen-Poiseille equation [44]:

$$\Phi = \frac{\Delta P}{\Delta x} \frac{\pi R^4}{8\eta} \tag{4.1}$$

where R is the radius of the volume elements and η represents the viscosity. Its clear that the conditions 3. and 4. are fulfilled or can be easily fulfilled by the choice of calculation parameters. 2. can be dropped by taking the obtained results as boundary values, meaning that *we overestimate the flux and underestimate the time constants significantly.* This means, that the actual flux might be an order of magnitude lower, while the actual time constant might be an order of magnitude higher. This approximation is bold, as a noble gas is naturally highly compressible, however for checking the order of magnitude it is sufficient. We continue here with the ad hoc assumption that the predominant flow in such

a waveguide is laminar, given for a pressure of a few hundred *mbar* and having a core diameter of some hundred μm. According to reference [34, 33] this is the region of parameters where a maximization of the XUV output power is expected. It will turn out later that this assumption delivers self consistent results. Having the relation 4.1, we choose to refine our model such that the volume element V_i of constant pressure P_i is connected to its neighbors by a circular pipe of radius R and length Δx (see figure 4.8).

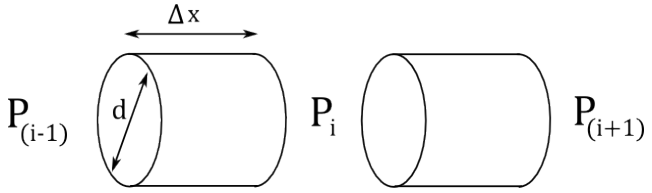

Figure 4.8: The volume element V_i at pressure P_i is assumed to be connected to V_{i-1} and V_{i+1} by identical pipes of diameter $d = 2R$ and length Δx

Assuming that the volume change can be related to a particle transport ΔN via the ideal gas equation:

$$\Delta N = \frac{P}{RT}\Delta V \tag{4.2}$$

where we assume P to be $P_{average}$ of the two adjacent volume elements. Therefore the change in pressure is given as

$$\Delta P = \frac{\Delta N R T}{V} \tag{4.3}$$

Considering the two contributions to the pressure of the i-th volume element, the instantaneous pressure change is given by:

$$\Delta P_i = \Delta P_{i-1\to i} + \Delta P_{i+1\to i} \tag{4.4}$$

Therefore

$$\begin{aligned}\Delta P_i = \Delta t \frac{R^2}{8\eta\Delta x^2}\Bigg[&\frac{P(i)+P(i-1)}{2}\left(P(i)-P(i-1)\right) \\ &+\frac{P(i)+P(i+1)}{2}\left(P(i)-P(i+1)\right)\Bigg]\end{aligned} \tag{4.5}$$

This can now easily be solved assuming the boundary conditions as depicted in figure 4.7, assuming that we know the pressure at the fiber end and that the pressure at the gas inlet is known. A good approximation for the pressure at the fiber tip is the expected pressure in the vacuum, for the simulations presented here it was assumed to be 10^-7 pa.The only thing that additionally needs to be known is the viscosity of the to be investigated gas. The simulations here were done with the value for Argon, being $22.9 \cdot 10^{-6}$ [pa s][45].

The explicit calculation works now like that: The boundaries are set to their appropriate values, then the pressure change can be calculated for all volume elements. After that the boundary volume elements are set back to their defined pressures and the next time step is calculated. It is important to take care that the used Δt is small compared to the time an atom would need to cross the volume elements. In this calculations this was fixed by requiring that $\Delta t \ll \frac{\Delta x}{v_{rms}}$, where v_{rms} is the rms velocity predicted by kinetic gas theory.

4.3.2 Temporal pressure evolution

The information that we want is whether or not the time constants involved in the pressure dynamics are comparable with the time constant of the consecutive laser pulses (100 ms) and in what order of magnitude the gas flux is that escapes into the vacuum. Figure 4.9 and 4.10 display the results of two example calculations. It is apparent that the time constant τ for reaching a steady state is one order lower than the laser repetition rate. According to this calculations, it would not yet be a problem for a fiber length of 6 cm with τ being in the order of 2.5 ms. Already for 8 cm fiber length τ is much larger than 5 ms for 80 μm fiber radius. Anyhow it has to be kept in mind that we underestimate the time constant, therefore it is reasonable to assume that the real time constants are infact longer than 10ms and be therefore in the order of the temporal pulse separation. Calculations including the compressibility of the investigated gas need to be done for clarification.

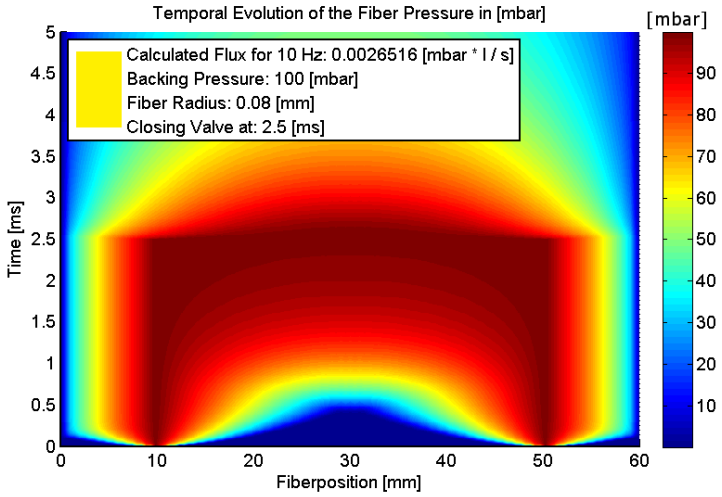

Figure 4.9: Pressure dynamics for Argon in a 6 cm waveguide with a core radius of $R = 80\,\mu m$

It was stated before that these simulations are self consistent in terms of the laminar flow assumption. This can be shown using the condition that the Reynolds Re number is at any time smaller than a boundary value Re_{crit}. For flow in a pipe this value is about 2000 [46]. The Reynolds number is now calculated as

$$Re = \frac{vR}{\eta}\rho \tag{4.6}$$

where v is the mean velocity of the atoms in the gas, R the radius of the pipe and ρ is the density of the gas. The above can be rewritten using Hagen-Poiseille formula form before.

$$Re(i) = \frac{r^3}{8\eta^2\Delta x}\frac{M}{RT}\Delta P_i \; P_{average} \tag{4.7}$$

here r was used for the radius in order to allow R as universal gas constant, M denotes the molar mass. Therewith we can plot a Reynolds map of every point in space and time and compare these values to Re_{crit}. Figure 4.11 shows these calculations for the data from figure 4.10.
The result here is, that the maximal value occurring is $Re_{max} = 300$, which is obtained at the first time step, where the boundary conditions, being step functions, can be regarded

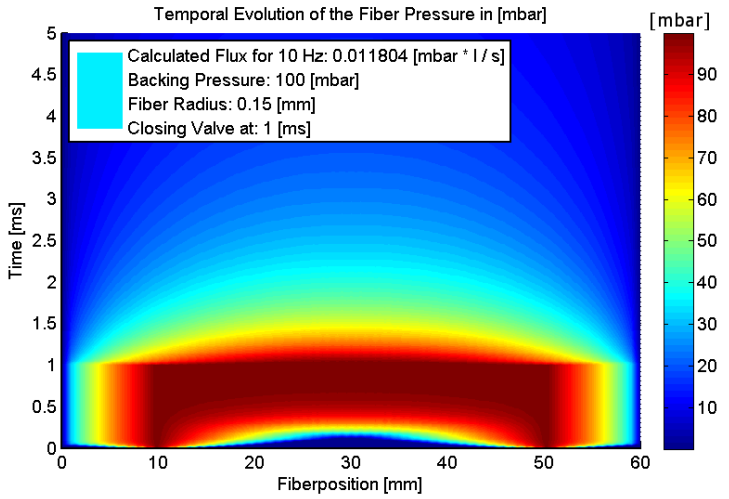

Figure 4.10: Pressure dynamics for Argon in a 6 cm waveguide with a core radius of $R = 150\,\mu m$

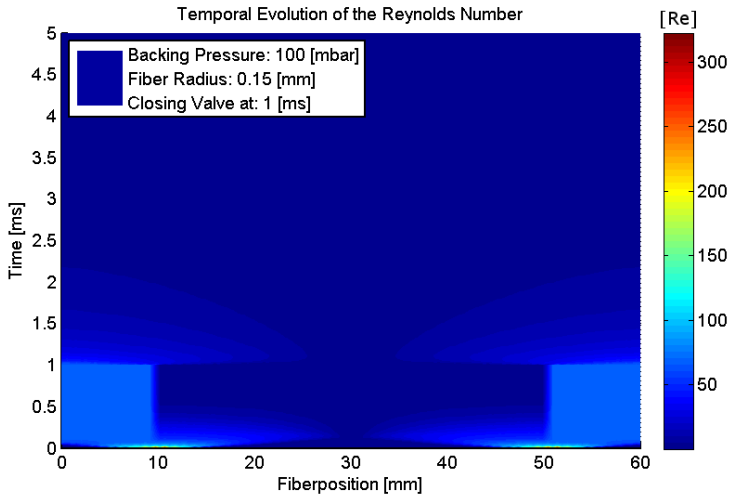

Figure 4.11: Reynolds map for Argon in a 6cm waveguide with a core radius of $R = 150\mu m$

as aphysical anyway. Therefore the simulations are for that set of parameters self consistent. For higher backing pressures, one runs into trouble at around 300 mbar for this fiber diameter.

4.3.3 Calculated gas flow into the vacuum

The model allows very easily to estimate the gas flow into vacuum, as for every time step the required pressure change of the inlet volume elements can be obtained. By summing over the quantity $\Delta P\, V$ for all time steps. The estimated leaking rate into the vacuum is then:

$$Q = f_{rep} \sum_t \Delta p(t) V \tag{4.8}$$

The gas flow is expected to depend at least in steady state only on the distance d between the gas inlets and the fiber opening. The steady state values should represent the expected leaking rates for the continuous gas flow case. Table 4.1 compiles the findings.

radius	steady state leaking rate $[\frac{mbar \cdot l}{s}]$ at 100 mbar	
	d = 1 cm	d = 2 cm
80 μm	0.08	0.05
120 μm	0.4	0.2
150 μm	0.9	0.5

Table 4.1: The leaking rates for the steady state case for two different positions of the gas inlet with regard to the fiber opening.

If we consider the dynamic case, where it is assumed that the gas flow is stopped shortly after the steady state is reached, significantly lower leaking rates are obtained. Table 4.2 lists the findings for two different fiber lengths. The corresponding time constants can be found in table 4.3.

radius	dynamic leaking rate $[\frac{mbar \cdot l}{s}]$ at 100 mbar and 10 Hz	
	fiber length: 6 cm	fiber length: 7 cm
80 μm	0.003	0.004
120 μm	0.006	0.009
150 μm	0.010	0.014

Table 4.2: The leaking rates for the dynamic case for different fiber lengths.

radius	τ $[ms]$ at 100 mbar	
	fiber length: 6 cm	fiber length: 7 cm
80μm	2.5	4
120μm	1.2	1.8
150μm	0.8	1.2

Table 4.3: The approximate time constant τ for different fiber lengths at 100 mbar backing pressure.

4.3.4 Conclusion

It has been shown in this section, that based on the given model dynamic gas supply to the fiber would seem possible, given the obtained time constants. The dynamic pumping

would reduce the gas flow by more than an order of magnitude for the critical $300\mu m$ fibers with the biggest continuous leaking rates.

However, the first choice to run the experiment would be with continuous gas flow as it is the most uncomplicated way to obtain a constant pressure profile. This is first of all because of the extenisve tubing that was required to connect the piezo valve with the fiber inlets. The timeconstants there would be dominating the system and make it very hard to predict the pressure distribution inside the fiber. Further due to the exclusion of the compression effects, the time constants have been underestimated. To make sure, that proper gas distributions are being reached more complicated calculations are required. Furthermore there is currently no possibility to directly measure the pressure distribution, that means in a dynamic gas flow setup there would be always a certain degree of uncertainty if the steady state is actually reached.

Finally this means, that if we are running into trouble with the continuous gas load, it would be better to change the pumping scheme in the vacuum chamber to a differential one instead of playing with the pulsed gas flow, as only that way the pressure profile can be guaranteed.

4.4 Outlook

This work sets the theoretical basis for a comparison of gas cells and hollow capillaries in terms of HHG efficiency and experimental handling. The next step is obviously to perform the experiments described in this thesis. If everything proceeds according to plan there will be beam time after the defense of this work. The most important things that need to be worked out before data can be collected, are the adaption of the current pressure system to our needs and the development of an appropriate alignment procedure. Both will be dealt with as soon as possible.

The immediate goal is then to characterize and quantify HHG in hollow capillaries and to compare the obtained data with literature [33, 34]. Optimum parameters in terms of pulse energy, intensity, capillary diameter, gas pressure and gas type will be optained in a multidimensional optimisation process. From these experiments we hope to obtain information about the transition from free focusing to wave guiding properties.

With the experimental results at hand, detailed analysis based on the described models will be conducted, hopefully allowing us to draw a conclusion in favor of either the free focusing gas cell geometry or the guided waveguide geometry.

Acknowledgements

The path of a human being is defined by the sum of the influences acting upon it. Without the influence of a lot of people this thesis would have never been written. Without a lot of people i would have never came to Sweden. Without a lot of people i would have maybe ended up in a totally different profession.

I want to thank Prof. Christoph Gerz for making me understand physics, Dr. Vladislav Yakovlev for showing me that i might have been a bit fast with that first conclusion and Prof. Anne L'Huillier for showing me that it does not matter, as long as you have fun working with it.

With the above being said, it was not less than an honor to work in the group of Anne L'Huillier. She provides an extraordinary working environment gathering an excellent set of people around her. Dr. Cord Arnold is possibly the best supervisor i could have ended up with. He left me all the freedom i needed to satisfy my curiosity while providing the required boundaries to actually move forward. Its also hard to underestimate the contribution of Diego Guenot to this work, he has the rare feature of having sufficient patience and genius to make an ordinary cobblestone understand quantum field theory. Filippo Campi generously supplied the punctuation for this thesis and the mutual exchange of insanities shall not be forgotten, it was a pleasure. I also want thank Esben Witting Larsen for the friendship and company, Piotr Rudawski for all the engineering help one could possibly ever imagine, David Kroon for the mustache, Kathrin Klünder for the music and being in general, Fernando Brizuela and Per Johnsson for their wonderful humor and Christoph Heyl for his patience under inquisitive questioning.

I want to thank my family. My grandmother for making the world a better place, my mother for supporting me since forever and my sister for being awesome. Without all of them this whole Sweden undertaking would not have been possible, financially and otherwise.

Bibliography

[1] Bransden and Joachain *Physics of Atoms and Molecules, 2nd ed.* Benjamin Cummings, 2003

[2] McPherson et al. *Studies of multiphoton production of vacuum-ultraviolet radiation in rare gases.* J. Opt. Soc. Am. B 4, 1987

[3] Ferray, L'Huillier, Li, Lompre and Mainfray *Multiple-harmonic conversion of 1064 nm radiation in rare gases.* J. Phys. B: At. Mol. Opt. Phys. 21, 1988

[4] Lewenstein et al. *Theory of high-harmonic generation by low-frequency laser fields.* Phys. Rev. A 49(3), 1994

[5] Lewenstein, Salieres and L'Huillier *Phase of the atomic polarization in high-order harmonic generation.* Phys. Rev. A 52(6), 1995

[6] Paul et al. *Observation of a train of attosecond pulses from high harmonic generation.* Science 292, 2001

[7] Krausz and Ivanov *Attosecond Physics* Reviews of Modern Physics 81, 2009

[8] Paul Corkum *Plasma Perspective on Strong-Field Multiphoton Ionization.* Phys. Rev. Lett. 71(13), 1993

[9] Rundquist et al. *Phase-Matched Generation of Coherent Soft X-rays.* Science 280, 1998

[10] von der Linde et al. *Generation of high-order harmonics from solid surfaces by intense femtosecond laser pulses.* Phys. Rev. A. 52(1), 1995

[11] Xiong and Chin *Tunnel ionization of potassium and xenon atoms in a high-intensity CO_2 laser radiation field* Sov. Phys. JETP 72(2), 1991

[12] Ivanov and Rzazewski *Are free-free transitions a good basis for nonlinear optics?* Journal of Modern Optics 39(12), 1992

[13] L'Huillier, Schafer and Kulander *Theoretical aspects of intense field harmonic generation.* J. Phys. B: At. Mol. Opt. Phys. 24, 1991

[14] L'Huillier, Balcou, Candel, Schafer and Kulander *Calculations of high-order harmonic-generation processes in xenon at 1064 nm.* Phys. Rev. A, 46(5), 1992

[15] L'Huillier et al *High-order harmonic-generation cutoff.* Phys. Rev. A, 48(5), 1993

[16] Antoine et al. *Theory of high-order harmonic generation by an ellyptically polarized laser field.* Phys. Rev. A, 53(3), 1996

[17] Li, L'Huillier, Ferray, Lompre and Mainfray *Multiple-harmonic generation in rare gases at high laser intensity.* Phys. Rev. A, 39(11), 1989

[18] Popmintchev et al *The attosecond nonilnear optics of bright coherent X-ray generation.* Nature Photonics 4, 2010

[19] Varju et al *Frequency chirp of harmonic and attosecond pulses.* Journal of Modern Optics 52 (2-3), 2005

[20] Balcou et al *Quantum-path analysis an phase-matching of high-order harmonic generation and high.order frequncy mixing processes in strong laser fields.* J. Phys. B: At. Mol. Opt. Phys. 32, 1999

[21] Lena Roos *Optimisation and Application of Intense High-Order Harmonic Pulses.* Dissertation, 2001

[22] Salieres et al. *Feynman's Path-Integral Approach for Intense-Laser-Atom Interactions.* Science 292, 2001

[23] D. M. Wolkow *Über eine Klasse von Lösungen der Diracschen Gleichung.* Zeitschrift für Physik A 94(3-4), 1935

[24] Bethe and Salpeter *Quantum Mechanics of One and Two Electron Atoms.* Springer, 1977

[25] Goldstein, Poole and Safko *Classical Mechanics, 3rd ed.* Addison Wesley, 2002

[26] Robert Boyd *Nonlinear Optics, 3rd ed.* Elsevier Science, 2008

[27] Katsunari Okamoto *Fundamentals of Optical Waveguides, 2nd ed.* Elsevier Science, 2006

[28] Julius Stratton *Electromagnetic Theory* McGraw-Hill Book Company, 1941

[29] John D. Jackson *Classical Electrodynamics, 3rd ed.* John Wiley & Sons, 1999

[30] Marcatili and Schmeltzer *Hollow Metallic and Dielectric Wave Guides for Long Distance Optical Transmission and Lasers.* The Bell System Technical Journal, July 1964

[31] Riley, Hobson and Bence *Mathematical Methods for Physics and Engineering, 3rd ed.* Cambridge Press, 2006

[32] Govind Agrawal *Nonlinear Fiber Optics, 3rd ed.* Academic Press, 2001

[33] Amy Lytle *Phase Matching and coherence of High-Order Harmonic Generation in Hollow Waveguides.* Dissertation, 2008

[34] Ariel Paul *Coherent EUV Light from High-Order Harmonic Generation: Enhancement and Applications to Lensless Diffraction Imaging.* Dissertation, 2007

[35] Baha Saleh, Malvin Teich *Fundamentals of Photonics, 2nd ed.* Wiley-Interscience, 2007

[36] Brabec and Krausz *Nonlinear Optical Pulse Propagation in the Single-Cycle Regime.* Phys. Rev. Lett. 78(17), 1997

[37] Kolesik, Moloney and Mlejnek *Unidirectional Optical Pulse Propagation Equation.* Phys. Rev. Lett. 89(28), 2002

[38] Courtois et al *Propagation of intense ultrashort laser pulses in a plasma filled capillary tube: Simulations and experiments.* Physics of Plasmas 8(7), 2001

[39] Skupin and Berge *Self-guiding of femtosecond light pulses in condensed media: Plasma generation versus chromatic dispersion.* Physica D 220, 2006

[40] Proch and Trickl *A highintensity multipurpose piezoelectric pulsed molecular beam source.* Rev. Sci. Instrum. 60(713), 1989

[41] Erik Mansten *Measurement and Control of Attosecond Light Fields.* Dissertation, 2009

[42] Erny et al. *Metrology of high-order harmonics for free-electron laser seeding.* New J. Phys 13, 2011

[43] Franck Wojda *Mesure de l'amplitude d'une onde de plasma crée par sillage laser guidé.* Dissertation, 2010

[44] Robert A. Granger *Fluid Mechanics* Dover Books, 1995

[45] *CRC Handbook of Chemistry and Physics, 92 ed.* Taylor and Francis

[46] Hof, Westerweel, Schneider and Eckhardt *Finite lifetime of turbulence in shear flows.* Nature 443 (59), 2006